Instrumentation Development, Measurement and Performance Evaluation of Environmental Technologies

Quarterly Technical Progress Report
for the period
January 1, 2002 - March 31, 2002

Dr. John Plodinec, Principal Investigator

Report No. 40395R15

Prepared for the U.S. Department of Energy
Agreement No. DE-FC26-98FT40395

Diagnostic Instrumentation and Analysis Laboratory
Mississippi State University
205 Research Boulevard
Starkville, Mississippi 39759-9734

dial@dial.msstate.edu
www.msstate.edu/Dept/DIAL

Notice

Table of Contents

List of Figures

List of Tables

Executive Summary

Characterization of Heavy Metals and Radionuclides

On-line isotopic monitoring and analytical protocol development for uranium and other actinides. A brief delay caused by the unavailability of replacement diodes for our external cavity diode laser (ECDL) has been resolved. Another laser vendor was located, allowing us to continue the CRDS portion of this effort. Cavity ringdown experimental efforts during this quarter have been directed at the high-resolution dye laser. Extensive usage has necessitated replacement of some optics. Baseline experiments to determine the isotopic resolution and sensitivity achievable for red-wavelength uranium transitions will begin upon completion of the required laser maintenance. During this reporting period, the LIF group's new moderately high-resolution dye laser system was successfully installed by the manufacturer. However, two visits (the first in February and the second at the end of March) by the manufacturer's representatives were required for successful installation; this delayed the start of our experiments with the new system.

Laser probe for technetium monitor. In order to enhance the sensitivity of LIBS for liquid samples, two different techniques were tested. First, we used two successive laser pulses to excite the sample. Second, we used different purge gases such as helium and argon around the liquid jet stream. The main aim of these experiments is to increase

the sensitivity of LIBS through a better coupling of laser energy to the target and ablated material leading to more efficient production of analyte atoms in the excited state. The calibration curve for Cr was obtained using both single-pulse and double pulse excitation techniques. LODs found from both cases were compared. The LOD of chromium changes from 1.3 ppm in the single pulse experiment to 0.12 ppm in double pulse excitation. Some initial results from the experiments with different purging gases show that the LIBS signal was enhanced more in the case of argon than in the case of helium or air. The signal in the case of helium, particularly the background emission, was suppressed in the presence of helium.

Development of Tools for Long-tern Monitoring

Monitor plant physiological status in contaminated environments by high-resolution spectral imaging. During this quarter, spectral and chemical analyses were done on diffuse reflectance spectra and harvested plant shoots from the first study of phytoremediation of Zn by barley (*Hordeum vulgare*); the growing portion of this study was conducted during the last quarter of 2001. Chemical analysis showed Zn accumulation in plant shoots from the two Zn-treated groups. Spectral analysis revealed a systematic difference between the near-infrared reflectance spectra of treated and untreated plants. In-depth spectral analysis suggested that band ratio of the spectral reflectance at 1110 nm compared to that at 810 nm might be used as an indicator of Zn accumulation in barley shoots. An extended abstract was accepted for oral presentation at the 9th Biennial International Conference on Nuclear and Hazardous Waste Management (Spectrum 2002).

Also during this quarter, we started the second study of phytoremediation of Zn and Cd by barley (*Hordeum vulgare*); this study will continue until May. Eight sub-groups (only three subgroups were used during the first study) of potted barley plants are growing and

will be treated with various concentrations of Zn and Cd solutions. Diffuse reflectance spectra with artificial illumination and with solar irradiation will be collected before and during the metal-treatment process. The plant shoots will be harvested and prepared for metal concentration analysis at the end of the study.

Moisture fiber-optic diode laser sensor (FODLS). The aim of this project is to achieve a fiber optic relative humidity sensor. Efforts in this period were:

- evaluating several polymers as coating material for moisture sensor construction,
- analyzing calibration behavior of $CoCl_2$/PVA coating of the bent probe for moisture sensing,
- evaluating LED as a light source for sensor construction.

Application of imaging techniques. One of the newly calibrated thermal imaging systems was successfully field deployed during a demonstration trip to Johns Manville's glass furnace in Etowah, TN. Work continued on system thermal calibration using various camera systems and on system software modifications for the thermal imaging systems with newly selected spectral regions.

The prototype of the grid-pattern projector for the WVNS melter inspection was completed. Fourier-transform profilometry (FTP) measurements of the projector's field-of-view and the area covered by different throw distances were also completed. A one-fourth-size model of the WVNS melter refractory core vessel assembly has been constructed (using 3/4-inch thick plywood). Initial FTP measurement results on this mock-up model showed detailed dimensions of all (five) planes that consist of the bottom section of core reaction chamber, but as an "inverted" target (the actual top appears to be bottom, and vice versa). Further investigation of the cause and remedy for this problem is underway. Software development, hardware design and construction of a prototype multi-axial remote controlled robotic system has started. The final mechanism will provide the necessary pre-

cision manipulation of the camera and projector needed to acquire images of the target surface remotely and accurately. Construction of a full-scale mock-up was also initiated.

As part of our spectral imaging effort, an acousto-optical tunable filter (AOTF) that enables us to select any arbitrary wavelength in the 500 to 1000-nm region was successfully tested, and computer software to control AOTF wavelength and data acquisition was developed and tested. We also made significant progress on improving the imaging acquisition and on-line processing software.

As part of the information-sifting component of this team effort, we began a comparison of spectral recognition using two different techniques: (1) principal component analysis (PCA), and (2) artificial neural networks. Preliminary PCA work using spectra from our plant-monitoring task indicated that PCA successfully identified spectra. This comparative study continues.

Hanford Tank Waste Chemistry

Saltcake dissolution and enhanced sludge washing. Components were obtained for the saltcake dissolution flow module (SDFM), and the system was assembled. Experiments with the ORNL base composition surrogate were conducted, and numerous difficulties associated with solids re-precipitation on the saltcake support filter and channeling through the filter were observed. Efforts were extended to locate filter media that was compatible with the supernatant composition. Poly(propylene) filters of 25 and 100-microns nominal pore sizes were tested and showed no signs of degradation due to caustic attack. Initial experimental results of the dissolution of the surrogate are presented. The results indicate that displacement of the saltcake supernatant from the pores of the salt matrix can take as long as ten hours for an initial volume of 300 cm^3 in the 3-inch diameter column. Viscosi-

ties measured during this period were within 10% of the supernatant or initial brine viscosity of 23 cP indicating little or no dissolution. Following the passage of the brine from the column, the viscosity was reduced dramatically. Calculations using the ESP model were performed.

Feed stability and transport: solids formation. Results are presented for the initial surrogate saltcake experiments using the saltcake dissolution flow module (SDFM). A significant length of time, 10 hours, was required for the effect of the diluent on the saltcake to be observed. During this period the effluent viscosity remained at or very near that measured on the undiluted surrogate supernatant. A second region followed wherein the viscosity was reduced and the chemical composition of the effluent changed. Nitrate, phosphate, and sulfate anion concentrations increased in accordance with dissolution of their respective salts. Aluminum and nitrite concentrations were reduced, and the chemical model correctly predicted this behavior. Results were in good agreement with the predictions from the ESP model with the exception of phosphate. The measured supernatant phosphate concentration was considerably less than the ESP prediction indicating that the model was not properly accounting for the partitioning between the phosphate in the liquid and the solid phases. Direct comparison to the model predictions indicated that only a 14% (by weight) extent of dilution was observed. Additional experimental plans are briefly described.

The CFD simulations on slurry transport have indicated that a regime consistent with the critical slowing down of a moving particle bed flow, eventually leading to an accumulation of particles, can be determined. The associated transition velocities were found to be linear functions of the average particle size and reduced particle density and the slurry (mixture) viscosity. Of these parameters the particle diameter and reduced density were found to influence the transitional velocity to a much greater extent than the slurry viscosity. Comparison of the determined velocities with empirical expressions for the

critical velocity, defined as that velocity at which the particle begins to undergo sedimentation, has allowed an initial assessment of the applicability of these expressions. The expression developed by Hudson and used to design the cross-site transfer line at Hanford results in a critical velocity 60% larger than the transition velocity obtained from the CFD simulations. Based on the simulation results, slurry transport operations at values of the Hudson critical velocity would not result in particle pile up or the eventual formation of a pipeline plug.

Environmental Control Device Testing

Evaluation of HEPA filter performance. The test matrices for Sections 4, 5 and 6 were developed as Excel files. These files were presented to the HEPA National Technical Work Group and discussed during a conference call on February 11, 2002. Particulate measurement instrumentation, including the ELPI, SMPS, and aerosol generators have been set up in the laboratory and interfaced to laptops and tested. Calibration data is being generated. These data will be included in a paper and presentation being made at the IT3 Conference in New Orleans during May.

Process Monitoring and Control of Toxic Organics

Sampling system for dioxins, furans and other semi-volatile products of incomplete combustion and characterization. The formation of dioxins and furans during combustion processes has become a significant focus of concern over the past few years. EPA has initiated an intensive effort to characterize the different sources of dioxins in the US and to reduce the overall annual rates of emissions. The 1999 MACT for Hazardous Waste Combustors establishes an emission limit for dioxins and furans that will be technically difficult to achieve. Large

strides toward controlling dioxin and furan emissions from combustion processes will most easily come from an enhanced understanding of their mechanisms of formation. The work being conducted by DIAL will seek to reduce uncertainties associated with the locus of formation of these compounds and factors that contribute to their formation.

Toxic organic compound monitoring using cavity ringdown spectroscopy. Much of the effort this quarter for the CRDS slit-jet expansion work focused on the construction of the vacuum system and its associated optical and mounting systems. The system was successfully vacuum-tested, and optimization of the pulsed slit valve operation is beginning. Additional efforts were directed at laser maintenance necessary after the transfer of the laser system from another location. Experimental work resumed for the diode laser CRDS system as well. This work is aimed at completing long wavelength scans of the C-H stretching vibration overtones for several volatile organic compounds. The DL-CRDS system was fully reassembled and realigned and is functioning well using the distributed feedback diode laser. The external cavity diode laser will likely require return to the manufacturer for further repair. A master's thesis in chemistry was completed and successfully defended in January based on work accomplished with the diode laser cavity ringdown system.

TASK 1

Characterization of Heavy Metals and Radionuclides

On-line Isotopic Monitoring and Analytical Protocol Development for Uranium and Other Actinides

D. L. Monts, Yi Su, C. B. Winstead, and T. Meaker

Introduction

Many DOE applications would significantly benefit from the availability of robust and convenient instrumentation for trace-level actinide monitoring and analysis. This project focuses upon developing new instrumentation for on-line or at-line monitoring for actinides with isotopic analysis capability. In addition, analytical protocols for a novel concentration method for actinides are being investigated. These efforts focus on demonstrating these techniques using uranium. In addition to its value in the analytical laboratory, the combination of a simple concentration technique with a robust isotopic monitor could provide a powerful method for addressing a number of outstanding DOE needs. Potential applications include monitors for wastewater and sewage treatment system influent and effluent and determining the isotopic content of transuranic species in low-activity waste fractions for waste classification and product acceptance. For example, the need for improved monitoring for uranium, plutonium, and americium in treatment plant influent is clearly identified in need

RF-ER11. With some additional sample pretreatment, such technology could also impact materials characterization needs by providing on-site isotopic analyses in a smaller and significantly less complex system than inductively coupled plasma mass spectrometry (ICP-MS).

The development of at-line or on-line monitors for uranium with isotopic analysis capability focuses on the evaluation of two laser techniques, laser-induced fluorescence (LIF) and cavity ringdown spectroscopy (CRDS), in combination with an inductively coupled plasma (ICP). The ICP serves as a sample atomization source, providing free uranium atoms and ions for LIF and CRDS measurements. For LIF, typical limits of detection (LODs) are on the order of parts-per-million (ppm) to parts-per-trillion (ppt), depending on the oscillator strength of the transition.[1] Thus, LIF has the required sensitivity to detect radionuclides at low concentrations. The use of high-resolution laser spectroscopy permits isotopic species to be differentiated from other isotopes of the same element. Because of the mass difference, the energy levels (and hence the absorption/emission wavelengths) of different isotopes are slightly shifted from one another. Combined with an optimized ICP source, LIF will address a DOE need for a rapid determination of concentrations and isotopic abundances of long-lived radionuclides in order to assure process control and product acceptance.

CRDS is a relatively new spectroscopic technique based on measurement of the decay time for laser light trapped in a stable optical cavity.[2] The presence of an absorbing species (such as uranium) in the cavity will reduce this decay time by absorbing some of the light propagating in the cavity. CRDS efforts toward isotopic uranium monitoring are focused on the construction of a small CRDS unit using diode lasers. These small lasers are available for some wavelengths in the blue region of the spectrum and most wavelengths in the red to near-infrared spectral region. They also possess an extremely narrow line width easily capable of isotopic resolution.

Our previous CRDS efforts using a narrow-line width pulsed dye laser have demonstrated isotopic resolution of mercury in an ICP, quantifying isotopic abundance features separated by as little as 1.1 pm.[3] These results suggest that a small, sensitive, and isotopically selective CRDS monitor is feasible. Our typical CRDS solution detection limits achieved thus far range from approximately one part-per-billion (ppb) for lead to 20 ppb for mercury.[3,4]

One need currently identified by DOE is the analysis of alpha emitters (U, Pu, Am, etc.) in wastewater effluents in the 10 nCi/mL range. This is typically done with either ICP-MS or alpha scintillation counting (ASC). An ICP-MS can cost several hundred thousand dollars and cannot distinguish between isotopes with similar masses (i.e. Pu-238 and U-238). ASC may require long counting times in order to detect isotopes with low disintegration energies. Reaching detection limits of the caliber of ICP-MS on a low cost instrument ($50,000 to $75,000) could be greatly facilitated using efficient concentration mechanisms. Currently, materials are available that can extract uranium and other actinides from water matrices. After extraction, actinides are eluted from the concentration media via concentrated acids (ranging from a couple of weight percent to 3 M). The concentration media are typically in the form of coated particles that are mixed with a volume of sample (1 - 2 L) and filtered prior to eluting with acid. These concentration methods are not particularly user friendly. The 3M Company has developed concentration disks for the extraction of transition metals and radioactive Cs, Sr and Tc. They are currently working on extraction disks for actinides. By using extraction disks, a volume of sample can be passed through the disk similar to filtration. Although this eliminates one step from the coated particle concentration scenario, the ultimate concentration method would simply contact the sample with an extraction tool that would double as an injection device similar to solid phase micro-extraction (SPME) on GC/MS. These preconcentration methods will be evaluated using LIF or CRDS techniques as well.

Work Accomplished

Laser-induced Fluorescence Spectrometry

During 2001, the LIF group placed an order for a moderately high-resolution dye laser system that was finally delivered at the beginning of January 2002. This dye laser system is required to enable us to have the required spectral resolution and not have to rely upon when we can borrow the CRDS group's laser. Arrangements were then made with the manufacturer for the installation of the new laser system. During February, the manufacturer's installers visited DIAL and attempted to install the dye laser. The installers were able to optically align the dye laser and achieve lasing. However they were unable to correctly synchronize the motion of the line-narrowing etalon with the dye laser wavelength scan; this is essential to provide us with tunability at the laser bandwidth required for successful resolution of uranium isotopes. The new dye laser system contains the first of a new generation of improvements in synchronized scanning technology. It was thought that the new version of the scanning software was the cause of the difficulty. At the end of March, the installers returned to DIAL. During their second effort, they discovered that some of the scan parameters in the dye laser's internal computer had been incorrectly set; once these parameters had been changed to the correct values, the correct synchronization between etalon and wavelength scan was achieved and the installation successfully completed. Because of the delay in installation of the new dye laser, our experiments were delayed.

Cavity Ringdown Spectroscopy

A brief delay was encountered for the uranium CRDS efforts during this quarter. The manufacturer has discontinued the external cavity diode laser (ECDL) to be used for these efforts, and new diodes are not available. A new diode will be required to continue our experiments using our existing ECDL. However, we were able to locate

another system that will allow us to continue this work. Cavity ringdown experimental efforts during this quarter have been directed toward the CRDS pulsed dye laser. Extensive usage has lead to the deterioration of some optics in the high-resolution pulsed dye laser. The laser is being realigned and recalibrated to compensate for this damage until replacement optics are received.

Work Planned

Laser-induced Fluorescence Spectrometry

Using the new laser system, we will continue our exploration of a variety of excitation/emission transition pairs in order to select the optimum excitation wavelength for isotopic abundance determinations. Efforts to purchase a spectrometer and intensified charged-coupled device (ICCD) detector for high-resolution detection of the uranium fluorescence have begun.

Cavity Ringdown Spectroscopy

As soon as the required laser maintenance is complete, baseline experiments to determine the isotopic resolution and sensitivity achievable for red-wavelength uranium transitions will begin. These experiments are paving the way for the development of a red wavelength diode laser CRDS system for isotopic measurements and will provide comparison data for previous CRDS studies of uranium using ultraviolet and blue transitions. The goal of this effort is to develop a small, diode laser-based system capable of isotopically resolved measurements of actinide species, such as uranium and plutonium.

References

1. X. Hou, S.J.J. Tsai, J.X. Zhou, K.X. Yang, R.F. Lonardo, and R.G. Michel. 1997. Laser-excited atomic fluorescence spectrometry: principles, instrumentation, and applications. In *Lasers in Analytical Atomic Spectroscopy,*

J. Sneddon, T.L. Thiem, and Y.I. Lee, eds., pp. 83-123. VCH Publishers, New York.

2. For example,
J.J. Scherer, J.B. Paul, A. O'Keefe, and R.J. Saykally. 1997. Cavity ringdown laser absorption spectroscopy: history, development, and application to pulsed molecular beams. *Chemical Reviews* 97:1:25-51.

G.P. Miller and C.B. Winstead. 2000. Cavity ringdown laser absorption spectroscopy. In *Encyclopedia of Analytical Chemistry*, R. A. Meyers, ed., pp. 10734-10750, John Wiley and Sons, Ltd., Chichester, England.

3. C. Wang, F.J. Mazzotti, G.P. Miller, and C.B. Winstead. ICP-CRDS: cavity ringdown spectroscopy as a plasma diagnostic. Submitted to *Applied Spectroscopy.*

4. F.J. Mazzotti, C. Wang, S. Tao, J. Mierzwa, C.B. Winstead, and G.P. Miller. Cavity ringdown spectroscopy for analytical mercury measurements. In preparation for submission to *Analytical Chemistry.*

Laser Probe for Technetium Monitor

V. N. Rai, F. Y. Yueh and J. P. Singh

Introduction

Technetium is a product of the nuclear power cycle. The most stable Tc isotope is ^{99}Tc. It has a half-life of 2.1 x 10^5 years and decays via β-emission. Due to the long half-life and the relatively high yield from uranium decay, DOE desires to separate technetium from non-radioactive and short life components of the tank waste. They plan to isolate it with other long life radionuclides in a geologically stable waste form for long term safe storage. An on-line monitor for technetium is needed for this waste processing. On-line monitoring during the waste processing will ensure Tc is properly removed from the processed effluent. The on-line Tc monitor should be able to measure

Tc below the 100-µg/L level. The technique should achieve at least a 10% confidence interval at 1000 µg/L.

This technical task focuses on the development and application of laser-induced breakdown spectroscopy (LIBS) to monitor Tc in effluent of Tc processing waste facility.[5] LIBS is a laser-based, non-intrusive, and sensitive optical diagnostic technique for measuring the concentration of various atomic and molecular species in test media.[6,7] It uses a high-power laser beam to produce a laser-induced plasma at the test point. The plasma atomizes and electronically excites the various atomic species present in the test volume in a single step. The intensities of the atomic emission lines observed in the LIBS spectrum are used to infer the concentration of the atomic species. LIBS has been successfully demonstrated its real-time monitoring capability in various field tests.[8-12] However, it is well known that the detection limit and precision achievable with LIBS can not yet surpass those of other analytical techniques. Various attempts have been made earlier to improve the analytical performance of the LIBS. We will evaluate various techniques, which can improve LIBS' sensitivity for Tc measurements.

Work Performed

The LIBS spectra of magnesium were recorded with the single and sequential double pulse LIBS systems. It was noted that the line emission intensity from the magnesium ion as well as the neutral atoms shows enhancement in the case of double pulse excitation. The enhancement in the line emission intensity was found dependent on various experimental parameters such as relative intensities of both the lasers, delay between the arrivals of the laser pulses on the target, the gate delay time after which the signal is being recorded as well as the concentration of the solution. For getting an optimum signal enhancement in double pulse excitation experiment, optimization of the parameters is necessary. Experiment was performed to see the

effect of delay between both the lasers on the LIBS signal. Figure 1 shows the variation in the intensity of line emission from magnesium ion at 279.55 and 280.27 nm and the neutral magnesium line emission at 285.2 nm. It was noted that LIBS signal from all the three lines increases with an increase in delay between the two lasers. LIBS signal increases till the delay reaches 2.5 - 3.0 µs. Further increase in the delay between the lasers shows decay in the LIBS signal. This signal was recorded at a gate delay of 10 µs in order to see the behavior of neutral line emission also, which remains absent at lower gate delay. The maximum enhancement in the signal was noted around ~6.5 times for the magnesium line emission at 279.55 nm. It was noted that ion line peak when the laser delay was between 2.5 - 3 µs, whereas neutral magnesium line peak at comparatively higher delay of 4 µs. It was also observed that neutral magnesium line intensity was initially (at lower delay) less than the intensity of ion lines. However neutral line emission dominates the ion emission, when delay between the lasers was greater than 10 µs. The dominance of neutral line emission was noted when the spectra was recorded at higher gate delay after the plasma formation, because at lower gate delay plasma remains hot and dense, which contains mainly electrons and ions. However, as the gate delay increases plasma becomes cool and the excited atoms (after recombination of electrons and ions) emit dominant radiation. Similar is the case when the delay between both the lasers is increased. Initially plasma is formed by the first laser, which expands normal to the target surface. The second laser beam interacts with the expanding plasma after certain time delay, which results in the plasma heating as a result of better absorption of the energy of the second laser in preformed plasma. This indicates that second laser beam excites the ions or the neutral atoms present in the plasma. If the delay in the arrival of second laser is small then mainly ions will be excited, whereas for higher delay neutral atoms will be dominantly excited. This confirms the emission patterns reported above.

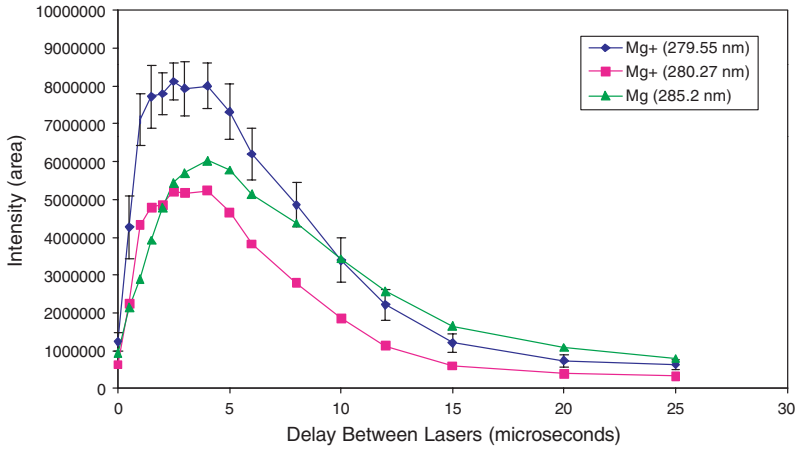

FIGURE 1. Double pulse LIBS signal from magnesium with delay between the two lasers.

The calibration curve of the chromium solution obtained using the single pulse and double pulse excitation techniques were compared and shown in Figure 2. The concentration of chromium was varied from 0.1 to 5 ppm and the limit of detection for Cr was calculated for both cases from the calibration curves. The LOD for Cr in double pulse excitation was found to be ~0.12 ppm in comparison to 1.30 ppm in the single pulse excitation. This shows that double pulse excitation improves the sensitivity of the LIBS system such that LOD of the elements (Cr) goes down by an order of magnitude.

In another effort to enhance the sensitivity of the LIBS system, argon and helium gas was used as purge gas around the liquid jet. Some of the preliminary results obtained from the single pulse LIBS of manganese in solution in the presence of argon and helium gas is shown in Figure 3. Comparing LIBS signal of manganese solution in air, we found that the argon environments shows an increase whereas in helium it decreases. Work to optimize the current system for this type of test is in progress.

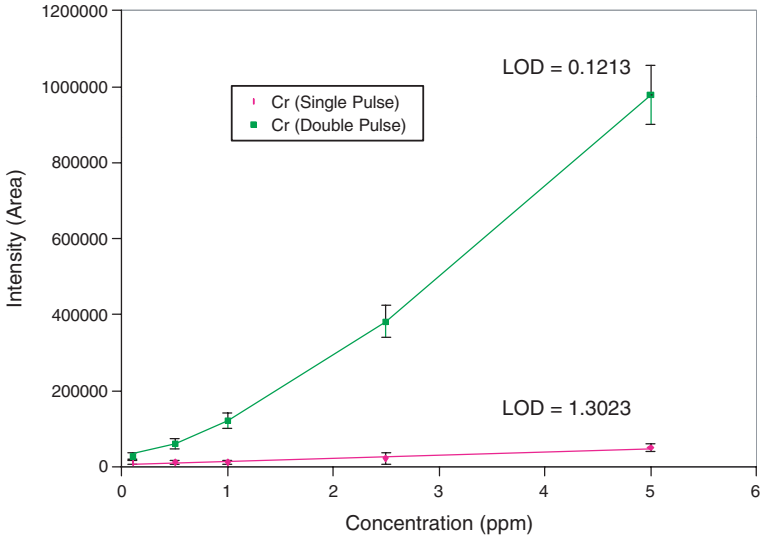

FIGURE 2. Comparison of calibration curve of chromium in solution recorded using single and double pulse LIBS.

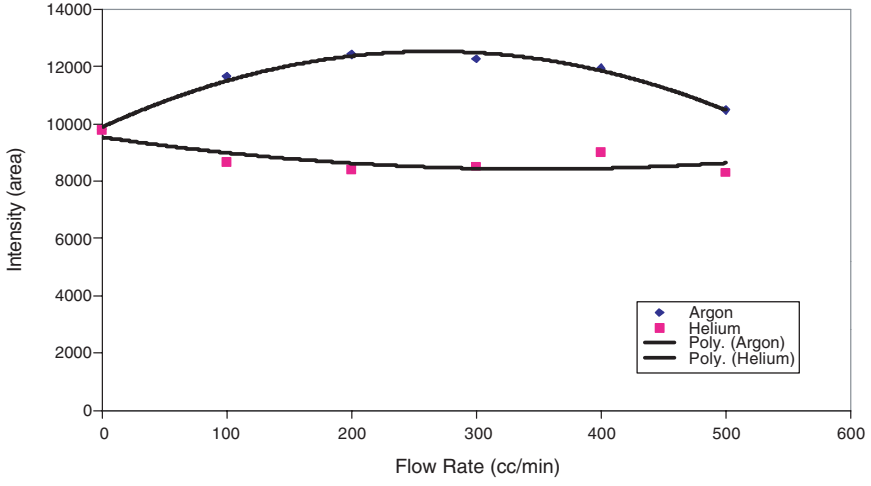

FIGURE 3. Variation in LIBS signal with flow rate of purge gases.

Work Planned

Experiments for optimization of the liquid measurement in different purging gases will continue.

References

5. F.Y. Yueh, R.C. Sharma, J.P. Singh, and H. Zhang. 2002. Evaluation of the potential of laser- induced breakdown spectroscopy for detection of trace element in liquid. Submitted to *Journal of the Air and Waste Management Association.*

6. F.Y. Yueh, J.P. Singh and H. Zhang. 2000. Elemental analysis with laser-induced breakdown spectroscopy. Invited chapter in *Encyclopedia of Analytical Chemistry: Instrumentation and Application*, pp. 2066-2087. Wiley, Chichester, UK.

7. L.J. Radziemski and D.A. Cremers. 1989. Spectrochemical analysis using plasma excitation. In *Laser Induced Plasmas and Applications,* L.J. Radziemski and D.A. Cremers, eds., Ch. 7, p. 295-326. Marcel Dekker, New York, NY.

8. J.P. Singh, F.Y. Yueh and H. Zhang. 1997. *Process control and quality,* 10:247.

9. J.P. Singh, H. Zhang, F.Y. Yueh, and K.P. Carney. 1996. *Applied Spectroscopy,* 50:764.

10. J.P. Singh, H. Zhang and F.Y. Yueh. 1996. Plasma arc centrifugal treatment PACT-6 slip stream test bed (SSTB) 100-hour duration controlled emission demonstration (CED) test. DIAL Trip Report 96-3.

11. H. Zhang, F.Y. Yueh and J.P. Singh. 1999. Laser-induced breakdown spectroscopy as a multi-metal continuous-emission monitor. *Applied Optic*s, 38:1459-1466.

12. H. Zhang, F. Y. Yueh and J. P. Singh. 2001. Performance evaluation of laser induced breakdown spectroscopy as a multi-metal continuous emission monitor. *Journal of the Air andWaste Management Association,* 51:174.

TASK 2

Development of Tools for Long-term Monitoring

Monitor Plant Physiological Status in Contaminated Environments by High-resolution Spectral Imaging

Yi Su and David Monts

Introduction

Purpose

The goal of this project is to use remotely sensed data to monitor the physiological status of plants growing on contaminated DOE sites. The physiological status will be used as an indicator of the presence of pollutants, such as heavy metals or radioactive species, in the growing environment. This capability will enhance DOE's capability for cost-effective long-term monitoring of contaminated sites.

Plant reflectance is governed by leaf surface properties and internal structure, as well as by the concentration and distribution of biochemical components, and thus remote analysis of reflected light can be used to assess both the biomass and the physiological status of a plant. Particular spectral bands and band combinations (often referred as reflectance indices) for monitoring crop stress resulting from nitrogen deficiency, water deficiency, etc. have been reported using remote

sensing. We propose to monitor the impact of contamination, such as heavy metals, on plant physiological status. A computerized spectral imaging system will be applied to take images of plants growing in a controlled environment with known concentrations of heavy metal contamination. Spatial and temporally distributed information extracted from images of different spectral bands will be part of this plant physiology study. The focus of this project is to search for indices (signatures) that indicate the impact and the content of heavy metals in the leaves and canopies of live plants. This ground-level study will also help to determine whether the physiological reflectance signals are stronger than disturbances introduced by factors such as the position of the sun, heterogeneity of the landscape, or atmospheric interference. The resulting information will be essential to determine whether remote sensing technology can be used for long-term monitoring of the spread of pollutants at some of the DOE closed sites.

Methodology

A portable spectroradiometer system and a spectral imaging system will be applied to monitor plant physiological status in contaminated environment. The spectroradiometer will be used to record reflectance spectra from the plant throughout the growing process. The spectral analysis will provide us the impact of the contamination on the plant physiology, and also will help determine the key spectral band(s) (signature) related to specific contamination. A spectral imaging system, which is based on the outcome of Task 3.2 (On-Line Multispectral Imaging of Thermal Treatment Process) of last year's Cooperative Agreement, will provide the spatial analysis. The spectral imaging system will help us overcome problems related to mixtures in the field of view, such as soil, dry leaves, stems, and shadows. The information extracted from spectral images will also be used to study plant canopy structure change during the growing process.

This is a multi-year project. First year will be devoted to a laboratory study: a laboratory-size plant bed will be used to study the

impact of selected metal species on plant physiology status. The second and third years will be devoted to study plants grown under a controlled natural environment for conditions similar to those that pertain to selected DOE sites; the plants affected by contamination will be studied in a potted-plant growing facility in a natural environment. The following years will be devoted to DOE site-specific studies.

Work Accomplished

During this quarter, we finished spectral and chemical analysis of the first study of phytoremediation of Zn by potted plants of barley (*Hordeum vulgare*). The growth portion of the experiment was conducted during the previous reporting period (from October to December 2001). Diffuse reflectance spectra (350 nm to 2500 nm) of the barley canopy were collected daily throughout the Zn-treatment process, a period of 22 days in total. The spectral data were analyzed using Microsoft Excel, after being converted to text files by software provided by the spectroradiometer manufacturer. Effort was continually made to ensure that the whole plant canopy area of each pot fell in the field-of-view of the instrument. The total of 24 pots of barley plants were randomly divided into three subgroups (T0, Zn T1, and Zn T2) with four barley plants in each pot. The first group of plants, T0, was provided with water only; the second group, Zn T1, was treated with 500 μM of Zn solution; and the third group, Zn T2, was treated with 50 mM of Zn solution. To overcome individual variability among barley plants, the reflectance spectra from each day were averaged within each of the three subgroups. As a result, each spectrum presented here is the average of reflectance of 32 individual plants. The laboratory reflectance spectra of the three subgroups are virtually identical before metal treatment was initiated. Figure 4 shows the laboratory reflectance spectra of the three subgroups on the day before, the 14th day, and the 20th day after the start of metal treatment. As can be seen in Figure 4, the reflectance spectra of the

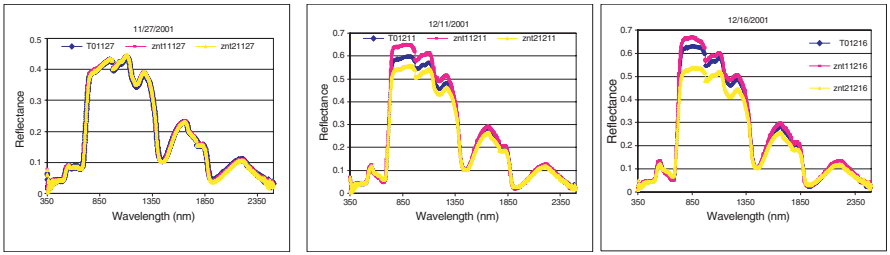

FIGURE 4. Diffuse reflectance spectra of potted barley plants from untreated (T0), ZnT1 and ZnT2 groups on the day before, the 14th day, and the 20th day after the start of Zn treatment.

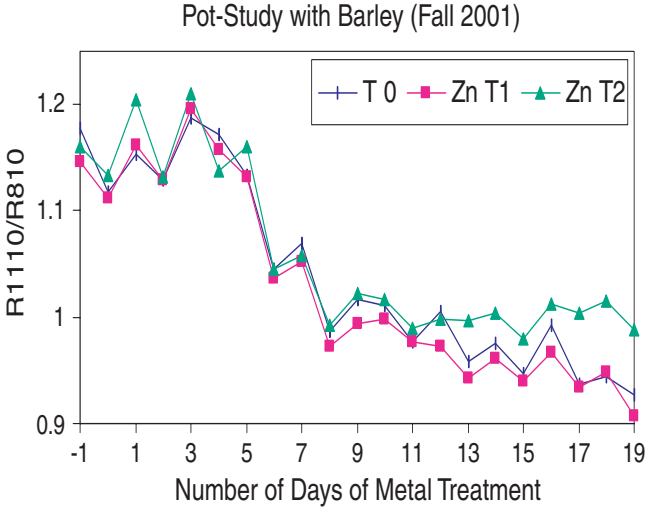

FIGURE 5. Band ratio R1110/R810 of three subgroups [T0 (untreated), ZnT1, and ZnT2] during and before the metal treatment process.

three subgroups are almost identical on the day before the start of Zn treatment. On the 14th and the 20th days after the start of metal treatment, the reflectance spectra of the Zn T2 subgroup are clearly differently from the T0 and Zn T1 groups. The spectra of the Zn T2 subgroup show differences in the near-IR region (from 800 nm to

1300 nm) consistently from the 14th day of Zn treatment. Because of the low Zn concentration (500 μM), the reflectance spectrum of the Zn T1 subgroup is very similar to the T0 subgroup. Further in-depth spectral analysis shows that the band ratio of the spectral reflectance at 1110 nm to that at 810 nm might be used as an indicator of metal accumulation in plant shoots. Figure 5 shows plots of the band ratio R1110/R810 for three subgroups [T0 (untreated), ZnT1, and ZnT2] during the metal treatment process. As shown in Figure 5, this band ratio distinguishes the three subgroups starting from the 13th day after the start of the metal treatment. We also observed reduced chlorophyll absorption at 680 nm when barley was exposed to high-concentration Zn solution. This observation is in agreement with the published literature.

TABLE 1. Accumulation of Zn in barley plant shoots (in mg/kg of plant dry weight).

Shoot #	T0	ZnT1	ZnT2
1	88	413	5500
2	166	627	10100
3	102	443	4190
4	72	407	6600
5	131	522	6440
6	136	572	7870
7	134	513	10000
8	110	370	3620

Analytical chemistry results on harvested plant shoots show Zn accumulation for the two subgroups treated with Zn solutions. The plants were cut about 2 cm above the soil at the end of the growth study. The harvested shoots were then dried at 80 C in an oven for 48 hours. Dry shoots were ground and weighed. Dried samples (0.3 g) were then dissolved in 7.0-mL aliquot of concentrated HNO_3 and a 3.5-mL aliquot of concentrated HCl. The samples were digested by

microwave, mixed with standard solution, and were analyzed for elemental composition using inductively coupled plasma-atomic emission spectrometry (ICP-AES). Table 1 shows the Zn accumulation in plant shoots of barley.

An extended abstract entitled "Monitoring the Process of Phytoremediation of Zinc by Barley *(Hordeum vulgare)* Using Visible and Near-Infrared Diffuse Reflectance Spectrometry" has been accepted for oral presentation at the 9th Biennial International Conference on Nuclear and Hazardous Waste Management (Spectrum 2002).

Work Planned

We have started the second study of phytoremediation of Zn and Cd by barley (*Hordeum vulgare);* the growth portion of this study will continue until May. Eight sub-groups (only three subgroups were used during the first study) of potted barley plants are growing and will be treated with various concentrations of Zn and Cd solutions. Diffuse reflectance spectra with artificial illumination and with solar irradiation will be collected before and during the metal-treatment process. The plant shoots will be harvested and prepared for metal concentration analysis at the end of the study.

Moisture Fiber-Optic Diode Laser Sensor

R. Jindal, S. Tao and J. P. Singh

Introduction

In our previous report, a bent fiber probe coated with $CoCl_2$/PVA was tested for sensing humidity. The bent probe was verified to response to humidity change down to 5% relative humidity at room

temperature. To reach the goal of constructing humidity sensor for sensing soil moisture or down-hole humidity, there are still some problems need to be solved. Efforts in this period deals with some of the problems. These efforts bring us closer to our goal.

Work Accomplished

Evaluate Polymers as Coating Material for Moisture Sensor Construction

The response of a bent fiber probe coated with different polymer to moisture change is studied. In this work, three polymers (sol-gel silica, PVA, PMMA) were tested as coating material for constructing coating based moisture sensor. The property of these polymers is significantly different. Sol-gel silica is a porous hydrophilic polymer. PVA is a hydrophilic polymer and PMMA is a hydrophobic polymer. Pure polymer coating and polymer doped with indicator ($CoCl_2$) coating on bent fiber were tested as moisture sensor. Test results show: (1) a bent probe coated with pure sol-gel silica responses to moisture change with moderate sensitivity; (2) a bent probe coated with pure PVA or pure PMMA does not response to moisture change; (3) a bent probe coated with $CoCl_2$/PVA responses to moisture change with high dynamics; (4) a bent probe coated with $CoCl_2$/PMMA responses to moisture change with limited sensitivity. From these test result, two coatings (pure sol-gel silica and $CoCl_2$/PVA) can be used to construct moisture sensor.

Calibration Behavior of $CoCl_2$/PVA Coating Based Moisture Sensor

Calibration behavior of $CoCl_2$/PVA coating based sensor for moisture sensing was studied. The response of a bent probe coated with $CoCl_2$/PVA to moisture was tested by exposing the sensor to air gas with certain moisture for a long enough time. The relationship of

the output of the sensor in dB to moisture content in air was established. A linear relationship between the dB and the RH% is available in a certain humidity range. Theoretically, a linear calibration curve is not available in wide humidity range for a fiber optical moisture sensor with $CoCl_2$ as an indicator and a He-Ne laser (632 nm) as a light source. This is because the absorption signal of $CoCl_2$ is monitored in this sensor, while the humidity content is proportional to the concentration of $CoCl_2.6H_2O$. The concentration of $CoCl_2.6H_2O$ in the polymer can not be directly monitored through light absorption measurement, because $CoCl_2$ also absorbs light at the wavelength $CoCl_2.6H_2O$ have peak absorption (at around 550 nm). In practical applications, a linear calibration can be achieved for a certain humidity range through adjusting the concentration of $CoCl_2$ in the coating.

Possibility of Utilizing Light Emitting Diode (LED) as Light Source for the Moisture Sensor

LED is small in size, cheap, simple and has a very long lifetime. In addition, a LED can be powered by using a small battery (2 - 4 V). Therefore, utilization of LED as light source in fiber optical moisture sensor design will reduce the cost of the sensor (an LED usually costs less than a quarter of a dollar) and make the sensor simple. In addition, the sensor can be deployed to some remote area since it can be powered with battery. Preliminary test with a red LED (peak emission at around 670 nm) as light source for a bent probe sensor gives satisfactory result. The light intensity from the LED is high enough for a photodiode array detector.

Work Planned

Further work will be focused on:

- Pure sol-gel coating for moisture sensing. Coating condition, such as fiber pretreatment, sol solution concentration, gelating time before coating, etc., will be optimized.

- $CoCl_2$/PVA coating based sensor. The $CoCl_2$/PVA coating based sensor needs a protecting package. Polymer based packing will be tested.
- LED as light source for sensor construction. Device for directly coupling light from a battery powered LED to fiber will be constructed.

Application of Imaging Techniques

D. L. Monts, Yi Su, P. R. Jang, and T. Philip

Introduction

Methodology

Our efforts will concentrate on DOE needs for inspection of off-line Joule-heated melters to determine wear patterns and the location and composition of deposits; this information can be utilized in the design of the next generation of HLW melters. Narrow bandpass filters will be combined with block cameras to enable spectral imaging within the melter. DIAL's imaging capability will be extended to the near-infrared spectral region. Diffuse reflectance spectroscopy will permit selection of proper observation wavelengths. Means of quantitative determining the extent of wear or amount of deposition will also be developed based on two techniques: Fourier transform profilometry (FTP) and stereovision. DIAL has previously demonstrated that its FTP system can quantitatively determine the volume and depth of removed material to high accuracy. Improvements will include (1) improvement of the fringe pattern projection system and (2) improvement of the phase unwrapping algorithm-this upgrade will resolve the 2 π-phase discontinuities associated with abrupt changes in surface height. A second imaging technique, stereovision, will also be developed as a means of determining the depths/heights

of surface features. Stereovision provides determinations of depths/heights by combining images simultaneously recorded by two cameras. Knowledge gained from and techniques developed for characterization of off-line melters can also be applied to characterization of on-line melters. A collaborative arrangement has been established with SRS's DWPF facility to inspect their melter at an appropriate time. Efforts are underway to establish a similar relationship with West Valley.

Techniques have been developed to detect hot spots, thermal distribution, characterization of vegetation, detection of uneven surfaces, etc. from imaging data. This year's effort also aims at enhancing the techniques already developed here and to develop new techniques and capabilities utilizing statistical as well as intelligent system approaches. While statistical methods provide linear relationships, artificial neural networks are apt to deal with non-linear relationships inherent in the data. Besides these, rule-based techniques would derive heuristic relationships. The existing capabilities will be extended to characterize soil, melters, and vegetation from uni- and multi-spectral images. This will enable long-term monitoring to detect the presence and variation of trace elements, especially hazardous ones in plants. The ability to classify regions of interesting characteristics will provide valuable information regarding contamination in soil and other media. One of the objectives of this effort is to go beyond typical data analysis methods in pursuit of discovering new relationships and thereby sifting information hidden in the data.

Work Accomplished

Profilometry

The prototype of the grid-pattern projector for the WVNS melter inspection has been completed. Measurements of the projector's field-of-view and the area covered by different throw distances have also been completed. As shown in Figures 6 and 7, a 3-D model CAD

drawing of the melter has been generated from West Valley's blueprints and a one-fifth-scale foam model has been build. Field-of-views from the port openings can be easily obtained through manipulation of the CAD drawing.

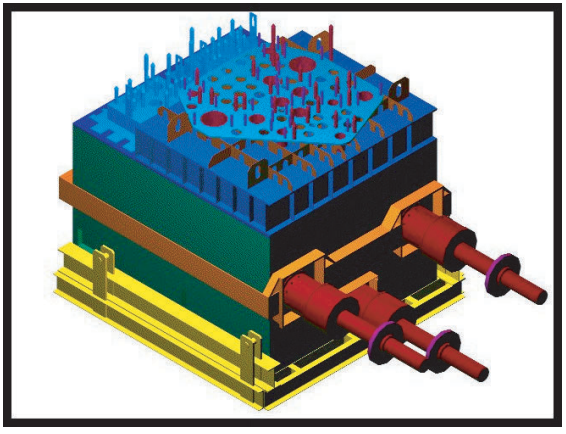

FIGURE 6. Computer-generated 3-D CAD drawing of WVNS melter from West Valley's blueprints.

FIGURE 7. One-fifth-scale foam model of WVNS melter.

Construction of a full-scale mock-up was also initiated. In Figure 8, a one-fourth-scale model of the WVNS melter refractory core vessel assembly has been made (in three quarter inch thick plywood).

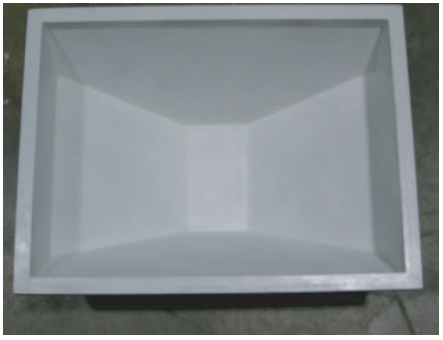

FIGURE 8. One-fourth-scale mock-up of WVNS melter core assembly.

Initial FTP measurement results using this mock-up model show detail dimensions of all (five) planes that consist of the bottom section of core reaction chamber, but as an "inverted" target (the actual top appears to be bottom, and vice versa) as in the Figure 9.

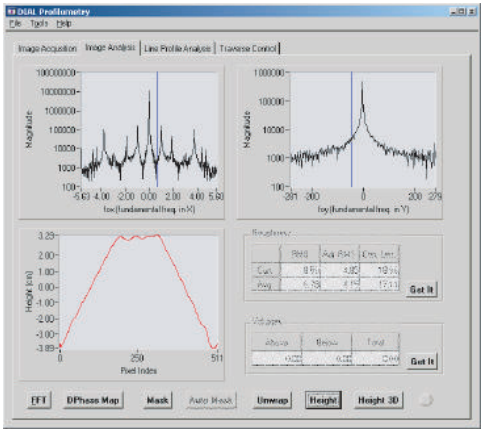

FIGURE 9. Initial FTP measurements result in inverted target height.

Further investigation of the cause and remedy for this inversion problem is underway.

The software development, hardware design, and construction of a prototype multi-axial remote controlled robotic system have been started. The final mechanism will provide the necessary precision manipulation of the camera and projector needed to acquire images of the target surface remotely and accurately.

Thermal Imaging

A closed-circuit TV (CCTV) system made by CombustionTec/Eclipse was modified by DIAL's Thermal Imaging group so that the system will not only provide visual monitoring inside a high-temperature furnace, but also provide thermal distribution information at critical locations. A joint field demonstration with the DIAL Thermal Imaging group and the CCTV system developers from Combustion Tec/Eclipse to a glass furnace in Etowah, TN has been successfully performed. During the demonstration, notes were taken by the facility operators, pointing out where the facility operation can be improved by looking at the "live" (near-real time) thermal information inside the glass furnace. Such notes include "if batch float is passing the bubble line", feed performance, thermal distribution along the wall refractory, etc.

As shown in the Figure 10, on the left hand side of screen, the original grayscale and false-color pictures are presented to the operator at 30 frames per second. These near-real time pictures provide an overview inside the glass furnace. On the right hand side, detailed information can be extracted by using the tools provided for a region-of-interest (ROI) selected by the user and drawn on the false-color image. In the figure, an oval area was selected. Its average temperature and intensity histogram are displayed. Also, a line was drawn on the charger wall horizontally between the two feed entrances. The temperature profile along the drawn line is also displayed. Again, all

of the imaging acquisition and imaging processing are completed within 1/30th of a second, which yields a “live” furnace monitoring and thermal presentation.

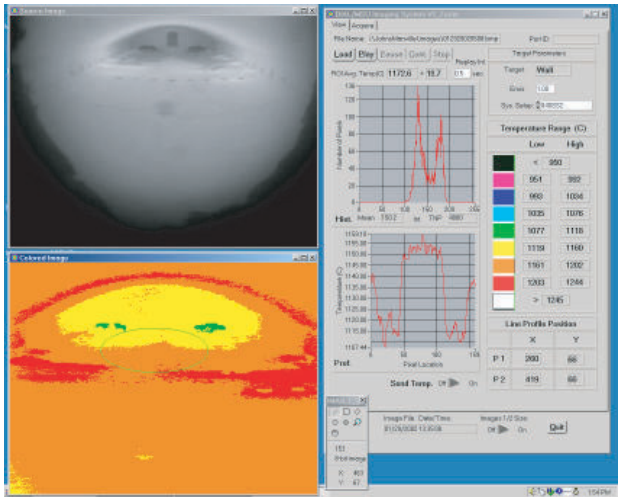

FIGURE 10. DIAL/MSU Thermal Imaging System with Eclipse CCTV System viewing inside glass furnace.

Further discussion with Combustion Tec/Eclipse and facility is needed to detail the wish list that facility may like to incorporate into the package. Possibility of bringing control loop into the system development will also be explored. Clearly this technology is directly applicable to process control of thermal treatment processes that are of interest to DOE.

Spectral Imaging

An acousto-optical tunable filter (AOTF) that enables us to select any arbitrary wavelength in the 500 to 1000 nm region was successfully tested and computer software to control AOTF wavelength and data acquisition has been developed and tested.

We also made significant progress on improving the imaging acquisition and on-line processing software. Experiments were performed on metal (uranium, europium, sodium, etc.) emission in an inductively coupled plasma (ICP) with the new imaging equipment and acquisition package in order to test the system. Results of these experiments have been used to improve the software package and were presented during this reporting period at the PittCon 2002 conference in a presentation entitled "A Multi-Species Spectral Imaging Study of an Argon Inductively Coupled Plasma (ICP)."[13]

Information Sifting

We have applied the principal component analysis (PCA) method to identify spectral data from plants and soil primarily to validate our model. A proximity index was used to indicate how close an unknown spectrum was to any one of the reference spectra. A value of zero for the index indicates exact match while values further away indicate the degree of dissimilarity. Our model performed well in assigning the proximity indices to the plant spectra. The data used was from the plant monitoring task and the spectral data was collected during summer 2001. We continue our validation efforts using soil data. An alternate approach using an artificial neural network needs further refinement.

Simple agent models were built using the AgentBuilder software tool. It works well in a single agent environment; however, we had trouble with multi-agent models. This effort is on hold for now and will be continued later.

Final manuscript of the paper "Characterizing thermal devices by identifying spectra using principal component analysis" by Thomas Philip, Yi Su, and David L. Monts was submitted for publication in the *Proceedings of the Computers and Their Applications (CATA-2002) Conference*.[14]

Work Planned

Profilometry

Work will continue on the study of the phase unwrapping algorithms[15,16] for target areas that have large height-discontinuities and/or surface isolations. Efforts will also continue on the full size mock-up system construction and the optical system control/delivery. FTP measurements of simulated surfaces inside WVNS melter will also continue.

Thermal Imaging

A new camera system, SONY XC-T50, has been identified. This camera system has better quantum efficiency than the existing camera and allows the camera exposure time (or electronic shutter speed) to be controlled by the width of an external trigger pulse. System development for the control scheme and thermal calibration will be followed. For the NIR InGaAs camera, system calibration against the blackbody will continue. The software module for reading parameters within PNG image file will be integrated with the current imaging system so that exact interpretation of acquired images can be achieved. We will continue the thermal calibration and system software modification for the new thermal imaging system with newly selected spectral regions and the high-resolution camera.

Spectral Imaging

During the next quarter, we expect to complete development and testing of the imaging acquisition and processing software package. We will then concentrate our efforts on development of a two-camera stereovision system. Also during this quarter, we will present a description of this task's melter autopsy efforts during a special session of the Annual Meeting of the American Ceramic Society.

Information Sifting

We plan to refine the artificial neural network approach as an alternative to the PCA method. We will explore ways to improve the speed of identification and also to build a data base for the spectral data. We will include soil data to the reference spectral library.

References

13. Yi Su and David L. Monts. March 2002. A multi-species spectral imaging study of an argon inductively coupled plasma (ICP). Pittsburgh Conference on Analytical Chemistry and Applied Spectroscopy (PITTCON 2002), New Orleans, LA.

14. Thomas Philip, Yi Su and David L. Monts. 2002. Characterizing thermal devices by identifying spectra using principal component analysis. Proceedings of 2002 Computers and the Applications Conference (CATA 2002), San Francisco, CA.

15. D.C. Ghiglia and M.D. Pritt. 1998. *Two-dimensional phase unwrapping*. John Wiley & Sons, Inc.

16. Yosuke Takahashi, Mitsuo Takeda, Masaya Kinoshita, Quan Gu, and Hideaki Takai. 1997. Frequency-multiplex Fourier-transform profilometry: a single shot three-dimensional shape measurement of objects with large height discontinuities and/or surface isolations. *Applied Optics* 36:22:5347-5354.

Acronyms

AOTF	acousto-optical tunable filter
CCTV	closed-circuit television
DWPF	Defense Waste Processing Facility
FTP	Fourier-transform profilometry

HLW	high-level waste
ICP	inductively coupled plasma
InGaAs	indium gallium arsenide
NIR	near infrared
PCA	principal component analysis
PNG	Portable Network Graphics
ROI	region of interest
SRS	Savannah River Site
WVNS	West Valley Nuclear Services

TASK 3

Hanford Tank Waste Chemistry

Saltcake Dissolution

R. Toghiani, J. Lindner, V. Phillips, and D. Selvaraj

Introduction

This project is a continuation of the work previously reported on the dissolution of Hanford waste saltcakes. A main portion of the work is to continually validate and upgrade a thermodynamic equilibrium model, the Environmental Simulation Program (ESP) as applied to the Hanford wastes. Toward this end, a number of significant accomplishments have been reported previously.[17-21] These include the evaluation of the code for the dissolution of saltcakes varying in composition through a comparison of model predictions with experimental results on core samples performed at the site, the use of the model to aid in the development of remediation strategies for Hanford tank 241-SY-101, an evaluation of data preprocessing, and the experimental determination of the solubility of natrophosphate, a double salt observed in the tank wastes.

A main focus is in bolstering the predictions of the code through comparison with experimental data and with other thermodynamic models such as SOLGASMIX. Accurate data called by the model are

an essential requirement for quantitative code predictions; however, it must be noted that evaluation of the thermodynamic interactions between all of the species existing in the waste streams is not possible. The path, therefore, has been to concentrate on those anions such as nitrate, nitrite, hydroxide, sulfate, phosphate, fluoride, oxalate, carbonate, and cations such as sodium, aluminum, calcium, nickel, uranium, etc., and the associate solids from these species that comprise the majority of the waste composition. Once assured that the code predictions accurately reflect the thermodynamics of these systems, it becomes possible to further upgrade the model to include other species of considerably lower concentration. The project is divided into three tasks as summarized below.

Task 1. Comparison of ESP to Other Thermodynamic Equilibrium Codes

The model has been shown to provide agreement with literature data for the solid liquid equilibrium behavior of many of the saltcake constituents at both high and low ionic strengths. Nonetheless questions will remain on the application of the model to situations where the ionic strength is high owing to the extrapolation of fundamental electrolyte theory to regions of high ionic strength. Theoretical calculations for sodium nitrate, the most prevalent solid in the waste, will be performed at high ionic strength and compared to an alternate model developed by M. Ally at ORNL. Comparisons with the SOLGASMIX model, in collaboration with C.F. Weber (ORNL) will be performed for the sodium-fluoride-sulfate system. Companion solubility experiments will be made on this system to improve the ESP database (Task 3).

Task 2. Comparison of ESP Predictions to Saltcake Dissolution Experiments

Previous work has characterized saltcakes with roughly four typical compositions as anticipated in the Hanford tank wastes. These

studies have indicated that ESP can be used to predict the dissolution behavior of the majority of the solids present. An exhaustive search for other types of saltcake compositions was conducted recently by D.L. Herting of Fluor Hanford resulting in the identification of two additional tanks with different composition distributions. A sample from tank TX-113 will be evaluated this year. In addition, recent interest in pretreatment and retrieval operations has indicated that there may be some concern when supernates from different waste streams are combined. ESP will be used to examine the propensity of solids formation under expected operating conditions. Predictions will be compared with on-going experimental work at the site.

A conference on the dissolution of saltcake will be organized and this forum will provide for extended discussions on the progress and results of the work and on future programmatic directions. Reports on the saltcake dissolution studies and on the outcomes of the saltcake dissolution conference will be provided.

Task 3. Improvements and User Documentation for the ESP Model

Some deficiencies have been shown to exist within the ESP databanks.[17] Of high interest is the determination of solubility data for double salts. Solubility studies for Na_3FSO_4 will be conducted and compared to the results of the prior literature and the calculations performed in Task 1. Additional studies on the extent of hydration as a function of ionic strength will be performed for Na_2CO_3 and Na_3PO_4.[22] Experiments are also planned for NaF at elevated ionic strength and in the presence of $NaNO_3$.

Considerable effort has been expended in learning the most appropriate ways in which to develop and run ESP simulations. These will be documented and forwarded to customers at Hanford for incorporation in the ESP User Manual.

Work Accomplished

Results and Discussion

Saltcake dissolution: modeling of experimental saltcake dissolution. Analytic data from the total sequential dissolution characterization on FY 02 saltcakes, B-109 and SX-101, were provided by D. Herting. These data were reconciled using Water Analyzer to generate a molecular stream for ESP input. The B-109 saltcake contains > 6% by weight fluoride, which is the highest level of fluoride examined in any saltcake tested thus far (total of eleven saltcakes over four year time period). It also contains ~ 23.2% by weight sulfate, which is also much higher than the highest sulfate level examined previously (~16.7% SO_4 by weight in saltcake TX-113). ESP predictions indicate a considerable amount of Na_3FSO_4 and of $Na_7F(PO_4)_2{\cdot}19H_2O$ to be present in the solid phase. ESP predictions of the percentage of each anion dissolved as a function of cumulative diluent addition are shown in Figure 11. The dissolution of fluoride and sulfate anions

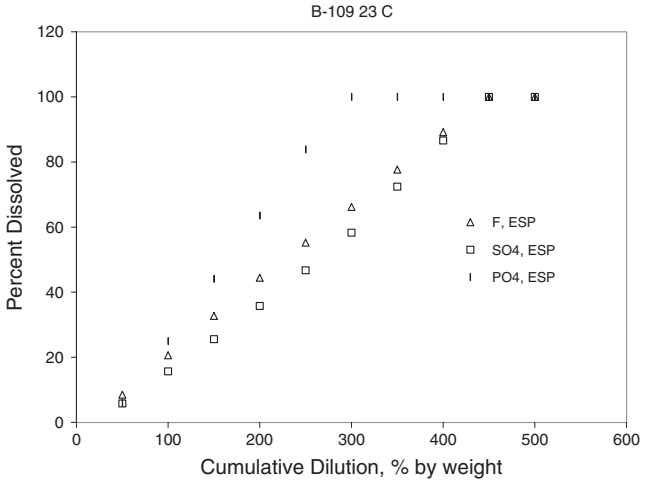

FIGURE 11. Dissolution profiles for sulfate, fluoride and phosphate for B-109 saltcake.

track one another closely. In Figure 12, the dissolution of the individual sodium salts is given as a function of cumulative diluent addition. The persistence of the sodium-fluoride-sulfate double salt in the solid phase is evident. Because of the high level of sulfate in this saltcake, this is an expected prediction. Solids characterization of the B-109 saltcake is planned and these predictions will be compared with the experimental data become available.

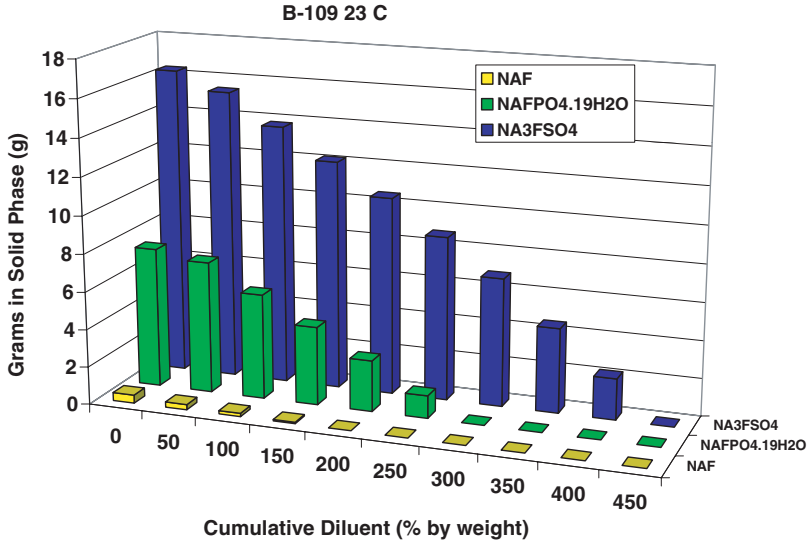

FIGURE 12. Predicted solids distribution for saltcake B-109 as a function of cumulative diluent addition.

Comparative calculations. ESP predictions of the sodium-carbonate-nitrate system at 25 C in aqueous solution were completed and are shown in Figure 13. The available literature data are also provided on this plot. ESP predictions were completed using: 1) only the PUBLIC database; and 2) using the PUBLIC database plus the TRONA database. Similar behavior to that observed previously for systems involving carbonate when the PUBLIC database only is used. Because the PUBLIC database does not allow the prediction of sodium carbonate monohydrate, there is a gap in the solubility envelope predicted using

the PUBLIC database only. When the TRONA database is used, the solubility envelope is predicted over the full range of nitrate concentrations. The solid phase predicted in the solutions with higher nitrate concentrations is the monohydrate of sodium carbonate. There is still a significant difference between the solubility envelope predicted by ESP (using the PUBLIC and TRONA databases) and the experimental data from the literature. This discrepancy is the reason for acquiring additional experimental data for this common ion ternary system. There is also no literature data available at temperatures other than 23 C and thus, additional measurements for the solubility envelope at 50 C will provide much needed experimental data upon which to base the interaction parameters for the carbonate-nitrate interaction.

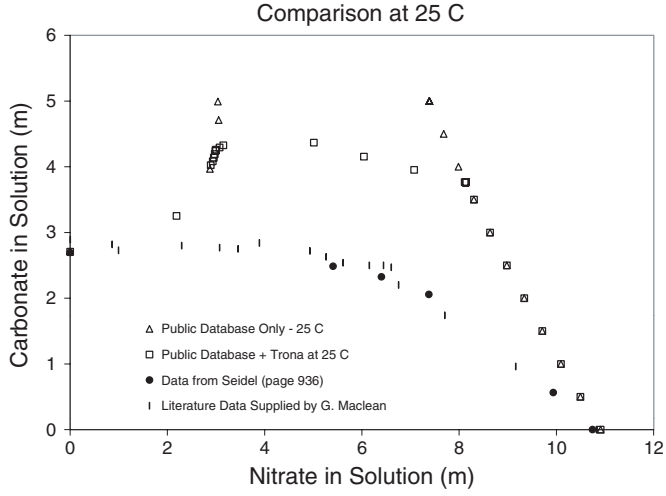

FIGURE 13. Solubility in the sodium-carbonate-nitrate system at 25 C.

Laboratory measurements for double salt systems. Experimental measurements for the solubility envelope in the sodium-fluoride-nitrate-phosphate-hydroxide system are nearing completion. Data regression is proceeding. Experimental measurements for the sodium-carbonate-sulfate-hydroxide system have been completed and regression of the data is underway. Experimental measurements for the sodium-car-

bonate-nitrate system in aqueous solution at 25 C are shown in Figure 14. The experimental data measured in this work are in good agreement with the available literature data and confirm that the ESP predictions for this system do not reflect the available experimental data in the region of moderate nitrate concentrations, 4 to 10-m nitrate. Experimental measurements for the sodium-carbonate-nitrate system in aqueous solution at 50 C have been competed and analytic results should be available in the near future. Comparison of these experimental data with ESP predictions will then be conducted.

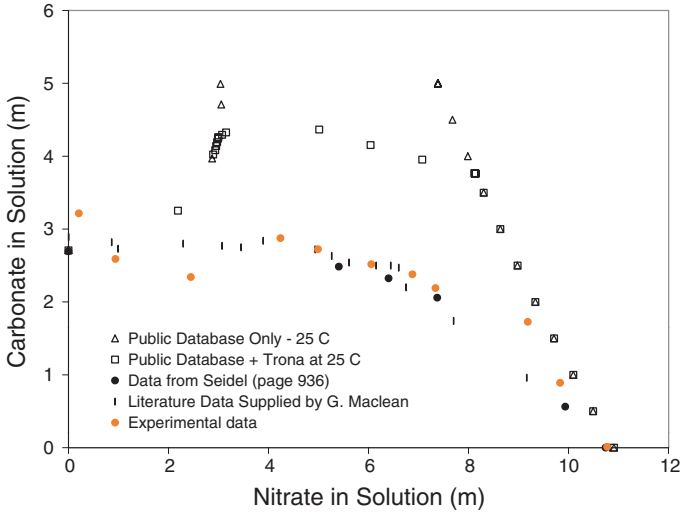

FIGURE 14. Experimental data for the sodium-carbonate-nitrate system at 25 C.

Conclusion

Experimental efforts have been focused on addressing the deficiencies in the ESP databases. These experimental data have been or, are in the process of being, regressed and will be incorporated into ESP.

Work Planned

Regression of available laboratory data will continue and compilation of regression results into a user-supplied database should be accomplished by the end of the second quarter of 2002. Revision of earlier predictions of saltcake dissolution will provide a point of comparison and reveal whether deficiencies previously noted are reduced and/or eliminated with use of the newly available data.

Laboratory measurements of the solubility for the sodium-fluoride-phosphate-nitrate-hydroxide system and sodium-nitrite-carbonate-hydroxide system are underway and will provide additional data in high ionic strength solutions.

References

17. R.K. Toghiani, J.S. Lindner, C. Barfield, and E.C. Beahm. 1998. Saltcake Dissolution Modeling, FY 1998 Status Report. DIAL-40395-TR98-1. Diagnostic Instrumentation and Analysis Laboratory, Mississippi State University, Mississippi State, MS.

18. R.K. Toghiani and J.S. Lindner. 1999. Saltcake Dissolution Modeling, FY 1999 Status Report. DIAL-40395-TR99-1. Diagnostic Instrumentation and Analysis Laboratory, Mississippi State University, Mississippi State, MS.

19. J.S. Lindner, R.K. Toghiani and C. Barfield. August 1998. Thermodynamic Simulation of Tank 241-SY-101 Dissolution, Part 1: In-Situ Crust Dissolution. DIAL 40395-TR98-1. Diagnostic Instrumentation and Analysis Laboratory, Mississippi State University, Mississippi State, MS.

20. J.S. Lindner and R.K Toghiani. October 1998. Thermodynamic Simulation of Tank 241-SY-101 Dissolution, Part 2:Supernate Transfer Followed by In-Tank Dilution. DIAL 40395-TR98-1.2. Diagnostic Instrumentation and Analysis Laboratory, Mississippi State University, Mississippi State, MS.

21. J.S. Lindner and R.K Toghiani. April 1999. Thermodynamic Simulation of Tank 241-SY-101 Dissolution, Part 3:Crust Solids Dissolution Modeling and Associated Gas Release. DIAL 40395-TR98-1.3. Diagnostic Instrumentation and Analysis laboratory, Mississippi State University, Mississippi State, MS.

22. D.L.Herting. October 1999. Personal communication.

Solids Formation

J. S. Lindner, A. Antonyraj, T. Durve, H. Al Habbash, and R. K. Toghiani

Introduction

Tank farm operations at Hanford include the interim stabilization program where the supernate and interstitial liquor in the single-shell tanks is reduced. Benefits from this process include the minimization of leakage from aging tanks, thereby limiting migration of waste into the soil, and the temporary reduction of waste within the tank. The process consists of jet-pumping the liquid in a given tank, obtained through a screen or salt well to a double-shell holding tank and then to an evaporator. Dilution water is added at the pump head. Recently, solids formation and plugging have been noted during transfers from tanks 241-SX-104, 241-U-103, and 241-BY-102.[23] The primary solid responsible for the plugs from the first two tank wastes has been tentatively assigned, through experiments conducted on the waste liquid in the laboratory, as $Na_3PO_4 \cdot 12H_2O$. The plug formed during salt well pumping of BY-102 was believed to arise from sodium carbonate.

Other solids may participate in the plug formation process and this will largely depend on the solid-liquid equilibrium of the species contained in the waste stream. Little information, aside from the laboratory screening experiments is known regarding the mechanisms of plug formation and, more importantly, the required change in pres-

sure that would indicate the beginning of plug formation. From operations measured records, the time needed for a plug can be determined and by knowing the pressures and flow rates the approximate location of the plug can be estimated; however, prevention of inadvertent plugs may be possible based on a suitable engineering tool that will allow operators to tailor waste transfers.

Long-term site operations will involve the dissolution of saltcake in the single-shell tanks and the removal of the salt liquor. Site plans are currently in progress for the retrieval of all of the salt in Hanford tank 241-S-112. Diluent will be added to the top of the saltcake followed by dissolution and permeation of the supernatant through the saltcake to the saltwell pump already located in the tank. Thus, some of the same problems that have already been addressed regarding the transport of high concentration phosphate solutions will remain. In addition, questions involve the rate and mechanisms associated with the saltcake dissolution process. These include the distribution of chemical species as retrieval proceeds (dissolution, dilution, and re-precipitation) and the physical characteristics of the saltcake bed, such as the porosity and permeability, which govern the rate at which the tank can be emptied. Work has started in this area with the development of an experimental approach that can provide the necessary information.

Work Accomplished

Support of 241-S-112 Saltcake Retrieval

Saltcake dissolution flow module (SDFM) functional experiments. The experimental design for the SDFM was presented previously.[24] The system was assembled and evaluated using the saltcake from the surrogate recipe developed by Hunt.[25] A number of problems relating to inadvertent solids formation on the stainless steel filter and within the exit plumbing were observed. Solids formed in the 300-micron pores of the filter as the droplets of the supernatant wet the stainless steel.

This effect tended to drastically reduce the throughput of the supernatant thereby altering the pressure across the column and the downstream flow rates. Subsequent determination of the porosities and permeabilities of the saltcake became questionable owing to filter blinding during experiment SC-8 and due to a faulty pressure transducer during experiment SC-9.

Efforts to re-design the bottom cap of the SDFM and to obtain a filter media that was hydrophobic were begun. Experiments could be conducted by developing a reservoir within the end cap and withdrawing the liquor near the top of the pool volume whereby the stainless steel filter would remain wet. Fouling was still observed and the use of the reservoir tended to unevenly mix the various supernatant fractions upon exiting the column. Discussions with filter manufacturers indicated that polypropylene (pp) units would provide pore diameters of up to 100 microns and resist the high caustic loadings. Filters with nominal pore diameters of 25 and 100 micron were received and evaluated.

Figure 15 shows the flow rate (cm^3/min) of water (as supplied by the peristaltic pump) through the filter. For these experiments the pp filter was positioned above a stainless steel grid of 1000-micron diameter pore size. This tended to add support for the flexible filter upon which the saltcake (density of 1.72 g/cm^3) would be placed. The flow rate was measured by weighing the fractions collected over a specific time increment and converting the weights to volumes using the known density of water. Four distinct regions are observed on the plot. The first corresponds to a region of no flow at the outlet of the column and was interpreted as wetting of the filter material. During this period the pump was on at the nominal 0.25 cm^3/min flow rate. Following saturation of the filter the measured flow rate rose rapidly to the flow rate of the pump and then remained constant until the pumping rate was increased. Another constant region was observed followed by lowering the flow rate to the original level and the attainment of a constant flow. Similar results were obtained when testing

the 25-micron pore diameter filter. The results, along with results presented below in connection with a dissolution experiment using the surrogate saltcake, indicate that the polypropylene filters are suitable for the experiment and that filter blinding does not occur.

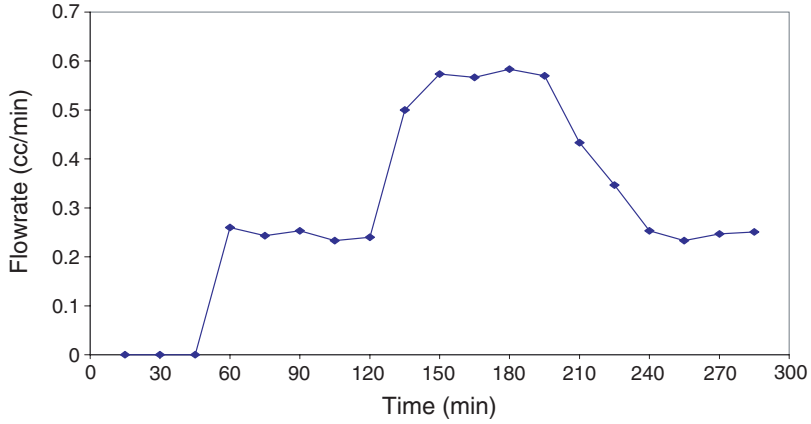

FIGURE 15. Measured flow rate at the outlet of the SDFM under different pump loads.

Experiments with the base composition surrogate - physical data. Tests with the surrogate composition were conducted using both the 300-micron pore diameter stainless steel filter with the modified, reservoir end cap, and with the polypropylene filter. For both experiments the diluent was water. Figure 16 illustrates the cumulative volume collected, divided by a factor of ten in both cases, and the average effluent viscosity against the run time.

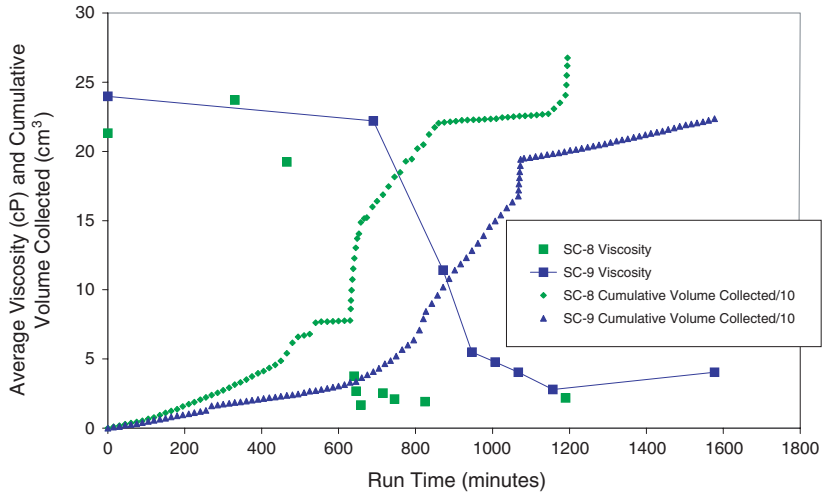

FIGURE 16. Average viscosities and cumulative volumes collected during the SC-8 and SC-9 experiments.

The general shape for the cumulative volume data for both runs is similar. Initially a regime is observed whereby the volume of supernatant collected is quite small. This corresponds to the period from the start of diluent addition to around 700 minutes of run time for the SC-9 (pp) experiment, and a slightly lesser time for the experiment with the stainless steel filter (SC-8).

The second region of the plot relates to a strong increase in the total volume of effluent collected. In the case of the SC-8 experiment the vertical increase in the cumulative volume observed 630 minutes into the run relates to an increase in effluent flow rate in some instances exceeding 1 cm^3/min, Figure 17. This value is around three times that of the inflow (0.3 cm^3/min).

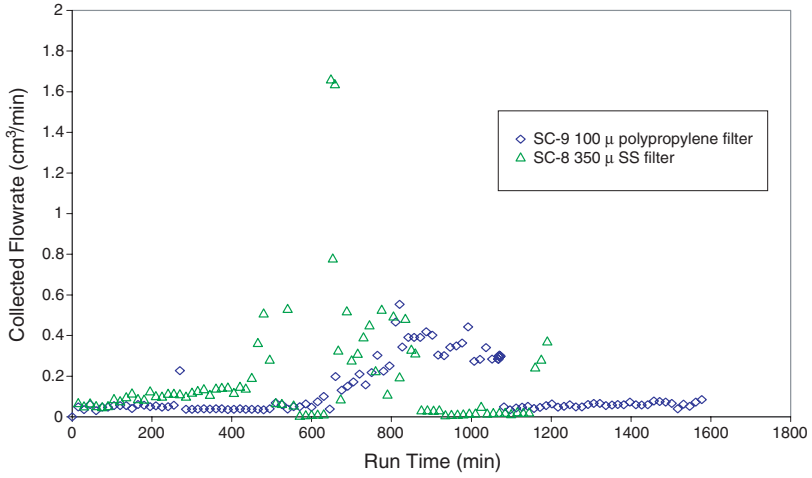

FIGURE 17. Effluent flow rates for the SC-8 and SC-9 experiments. Large increases in the flow rate represent channeling of the fluid through the bed.

The increase in the cumulative flow rate in the second region of Figure 16 was more gradual for the SC-9 experiment using the polymer filter. Extensive channeling was not observed here however the flow rates were seen to increase.

A third region in the data is observed at longer run times. Following the initial observation of channeling in the SC-8 experiment (at the run time of 630 minutes) the experiment was stopped. The remaining saltcake was withdrawn from the column and re-suspended. Examination of the stainless steel filter indicated an improper cut along the edge. A new filter was prepared and o-rings were placed both above and below the filter. The column was re-packed and the experiment continued. Dissolution continued to proceed until a large increase in the flow rate was observed at the end of the experiment. Only a small amount of saltcake remained and the metal filter was visible upon removing the top cap of the column.

Channeling was also observed around 1080 minutes for the SC-9 experiment. The third region of the plot for this experiment was similar to that of SC-8 with the exception that final channeling was not observed. In contrast to the operations performed during SC-8, the saltcake with diluent and supernatant was allowed to sit overnight prior to repacking the column. Additional solids were dissolved during this period and upon re-packing the column the bed height, as measured using the imaging system, was considerably reduced (see Fig. 18). Owing to this additional dissolution step any chemical composition data after 1080 minutes for SC-9 was determined as compromised.

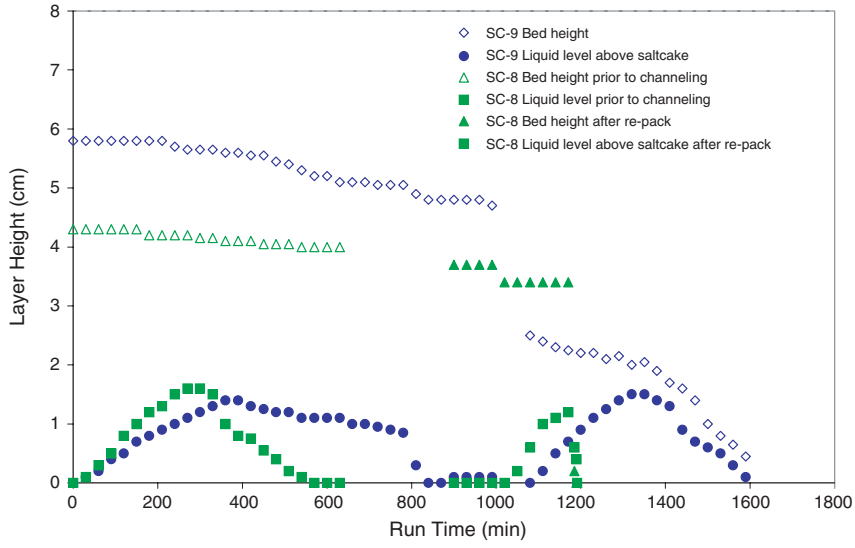

FIGURE 18. Salt bed heights and liquid levels above the salt bed.

The three regimes in Figure 16 are also broadly demarcated by the viscosity values measured for the effluent. In obtaining the 16-cm^3 volume required for these measurements a number of fractions were combined. Actual measurements were carried out at different shear rates with the rotational viscometer. In all cases and for all of the

samples evaluated, including the original supernatant or brine from the saltcake, the viscosities were strictly Newtonian. Values of the viscosity measured at different shear rates were then averaged and are plotted in Figure 16 against the run time for the last fraction collected.

It is anticipated that as bed dissolution continues the effluent viscosity will decrease. For both experiments the viscosities measured in region 1 were close to the measured viscosity of the saltcake brine, (21.3 and 23.9 cP respectively). These values remained reasonably constant for the SC-8 experiment until the run time approached 630 minutes. At this time the viscosity was observed to decrease from around 20 to 5 cP. The viscosity then continued to remain at the lower values until the conclusion of the experiment. More definition was observed in the results for SC-9. The viscosity decreased after a run time of 690 minutes reaching a value of 5 cP around 1000 minutes. The viscosity decreased gradually thereafter. The general trend in the effluent viscosities is most likely a sigmoidal response.

The initial (high viscosity) region in Figure 16 is consistent with the displacement of the original (non-diluted) brine or supernatant of the surrogate. A sufficient volume is still retained within the saltcake that, owing to the viscosity, requires considerable time to exit the bed. Sometime during the initial period the diluent begins to interact with the salt. This process is initially hindered by the high viscosity, high ionic strength brine. Salt bed heights and the liquid levels above the bed were measured using the imaging system and are shown in Figure 18. In this representation the liquid level above the saltcake has been corrected by subtraction of the saltcake height.

During the initial portions of the experiment, for example, for SC-8 until an elapsed run time of 450 minutes (prior to the observation of channeling), and for SC-9 until 690 minutes (corresponding to the still large viscosity at that point) the bed height decreases linearly and can be represented by

SC-8 Bed Height (cm) = (-0.6 x 10^{-3} cm/min)(run time, min) + 4.34 cm. **(EQ 1)**

The corresponding expression for the SC-9 experiment was

SC-9 Bed Height (cm) = (-1.1 x 10^{-3} cm/min)(run time, min) + 5.95 cm. **(EQ 2)**

It is clear that the initial dissolution rates are very slow. The change in the bed heights relates in the SC-8 experiment to a change in volume of 11 cm^3 in 450 minute or 7.5 hours. The change in bed height measured during the SC-9 experiment amounted to 32 cm^3 in the initial 690 minutes - both values translate to a decrease in bed volume of less than 3 cm^3/hour.

The data in Figure 18 for the saltcake bed height shows the continuation of the experiments. For the SC-8 run it was possible to re-pack the column without significant dissolution of the crystals and the run was continued although the chemical data following channeling was biased. Upon re-packing the saltcake for SC-9 the layer height was significantly reduced and for this reason the analysis of the chemical data for this run was confined to the first portion of the experiment.

Information on the ability of the diluent to permeate the saltcake is observed in the liquid levels shown in Figure 18. In both experiments the inflow was started at the flow rate of 0.3 cm^3/min. Shortly thereafter the liquid level was observed to rise. For the SC-8 and SC-9 experiments the total liquid level above the saltcake attained values of 1.6 and 1.4 cm, respectively. For the SC-8 experiment the pump was stopped at 360 minutes and for SC-9 the pump was stopped at 430 minutes and was re-started at 830 minutes. The pump was started again following the re-packing of the saltcakes and the liquid level again rose to greater than 1 cm above the bed height. Finally the inflow was turned off at 1380 minutes which roughly corresponds to the peak liquid level observed during the second phase of the SC-9 experiment.

The increasing liquid level above the saltcake indicates that the diluent flow is not completely permeating the salt bed. In the initial portion of the experiment the high viscosity of the base surrogate supernatant is believed responsible. Dissolution proceeded more rapidly in the later portion of the experiment but the saltcake could still not accept all of the diluent that was injected onto the column.

Experiments with the base composition surrogate - chemical data for SC-9. Diluted fractions collected during the SC-9 experiment were analyzed for nitrite, nitrate, sulfate, phosphate, and aluminum. All of the anions were determined using the ion chromatograph (IC) whereas the aluminum concentrations were determined using the inductively coupled plasma spectrometer (ICP). Multiple concentrations (traceable to NIST) were used to develop the appropriate calibration responses.

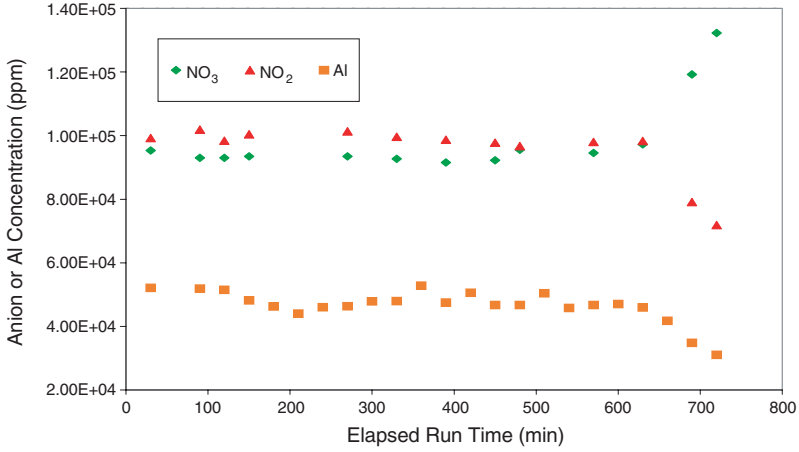

FIGURE 19. SC-9 effluent nitrate, nitrite, and aluminum concentrations.

Effluent concentrations for nitrite and nitrate anions and for aluminum are collected in Figure 19 and for sulfate and phosphate anions in Figure 20. Concentrations for all of the anions are essentially constant up to 630 minutes into the run. This behavior is consis-

tent with the near-constant values of the measured viscosity for the SC-9 sample and confirms that the effluent composition is not changing and that the composition is that of the original saltcake supernatant. After 630 minutes of run time specific trends corresponding with the dilution of the liquid phase (nitrite anion and aluminum) and subsequent dissolution of solids containing nitrate, sulfate and phosphate occur.

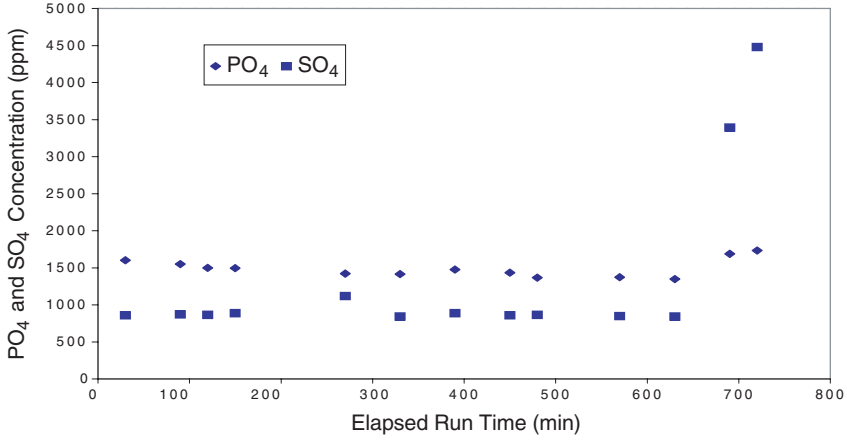

FIGURE 20. Concentrations of phosphate and sulfate anions during the SC-9 experiments.

The procedure for the preparation of the saltcake developed by Hunt at ORNL involves the development of a solution at 50 C followed by sequential additions of the ingredients such as not to result in an exothermic reaction.[25] Following dissolution of the components, the temperature of the mixture was then increased to greater than 100 C to evaporate water and then the mixture cooled to room temperature. One of the difficulties in preparation of the final saltcake composition is believed to be in the evaporation step. The temperature needed for boiling off the water is elevated. Thus, different lengths of time and different extents of mixing will result in saltcakes of slightly different water loadings. As opposed to the experimental procedure the ESP simulation will predict an equilibrium mass of water con-

verted to vapor at a given elevated temperature. Upon cooling the actual amount of water predicted to exist in the saltcake could be somewhat different from that of the preparation. ESP unit operations were performed to account for all of the preparation steps. In addition, a final component split was added so as to reduce the water in the predicted composition to the lowest loading where the model would still attain convergence. Summary ESP results (version 6.5 with the Trona and Na2Snacl databases) for the base composition saltcake and at different additions of water to this base composition are collected in Table 2.

TABLE 2. ESP predictions for the composition of the surrogate saltcake at 25 C.

% Dilution by wt.	0.00	13.97	27.85	41.77	55.70
Aqueous					
Temperature, C	25.00	24.13	20.90	16.69	12.92
H_2O(g)	232.79	400.53	560.04	715.31	871.13
Total (g)	568.29	841.88	1104.70	1347.20	1595.02
Volume (L)	0.37	0.56	0.75	0.92	1.10
Density (g/L)	1539.29	1495.96	1476.11	1457.03	1446.38
Abs Visc (cP)	18.94	14.55	13.06	11.92	11.21
pH	15.33	15.18	15.12	15.14	15.16
Ionic Strength	23.94	18.74	16.18	14.13	12.87
Solids (g)					
$Al(OH)_3$		15.09	23.32	28.52	31.42
$Na_2CO_3 \cdot 1H_2O$	67.70	28.09			
Na_2SO_4	14.62	13.71	11.62	5.98	
$NaNO_2$	11.32				
$NaNO_3$	353.25	282.02	195.70	107.52	17.65
$Na_3PO_4 \cdot 12H_2O \cdot 1/4NaOH$	112.34	104.24	106.19	109.32	111.45
Total (g)	559.24	443.15	336.84	251.34	160.53
Volume (L)	0.27	0.22	0.17	0.13	0.09

TABLE 2. ESP predictions for the composition of the surrogate saltcake at 25 C.

Density (g/L)	2063.65	2039.79	1984.46	1919.51	1791.52
Total Stream					
Total (g)	1127.53	1285.03	1441.54	1598.54	1755.55
Volume (L)	0.64	0.78	0.92	1.06	1.19
Density (g/L)	1761.25	1647.43	1570.10	1514.40	1472.31
% solids by wt.	49.60	34.49	23.37	15.72	9.14
% solids by vol.	42.33	27.85	18.49	12.40	7.51
% water by wt.	20.65	31.17	38.85	44.75	49.62

The initial composition was expected to contain 20% by weight water with an absolute viscosity of the liquid phase of ca. 19 cP. This value compares well with the measured viscosities of the SC-9 and SC-8 compositions, 23.9 and 21.3 cP, respectively. Samples for TGA determination of percent water have been submitted.

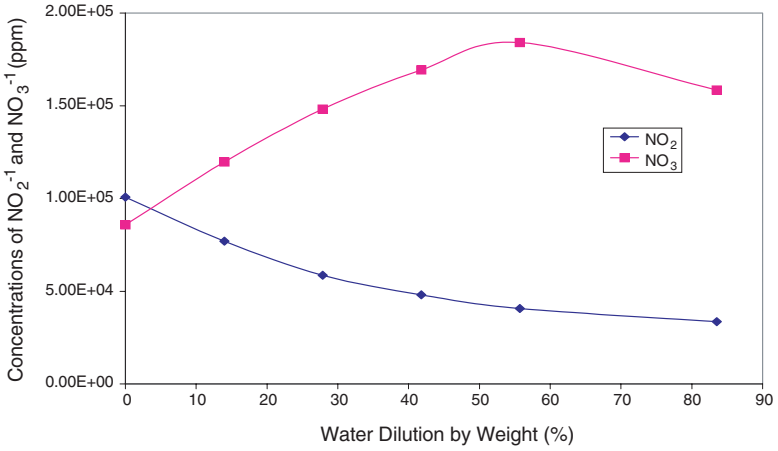

FIGURE 21. Predicted concentrations of NO_2^{-1} and NO_3^{-1} for the initial saltcake composition and at different levels of diluent (water) addition.

Predicted ionic concentrations for nitrite and nitrate anions are provided in Figure 21. Comparison with the experimental nitrate and nitrite anion concentrations (Fig. 19) reveals excellent agreement between the predicted values at 0 percent dilution by weight and the time period to 630 minutes into the experiment. Any dissolution occurring within the column is not revealed in the effluent composition in that time period. The model predicts an increase in nitrate loading, resulting from the dissolution of the large amount of sodium nitrate solids and a decrease in the nitrite concentration owing to direct dilution of the liquid phase constituent. The experimental results are in agreement with these trends.

Determination of the percent dilution achieved in the experiment is somewhat harbored by the channeling that was eventually observed around 1080 minutes. At a run time of 730 minutes, the determined concentration of nitrate was ca. 130,000 ppm and the concentration of nitrite was found to be 72,000 ppm. When compared to the simulation results these concentrations relate to a static dilution by weight of around 14%.

Model calculations for the phosphate and sulfate anions are shown in Figure 22. The phosphate concentration increases from an initial value of 4200 to 5170 ppm over an extent of dilution of 14%. Experimentally this value was observed to increase from 1460 to 1730 ppm. The similarity in the ratios of the two sets of data, 1.18 and 1.23 for the experimental and model predictions, respectively, provide further confirmation that the percent dilution achieved in the experiment was around 14%. Differences in the absolute values of the experiment and the ESP results are thought to reflect deficiencies in the model relating to the prediction of the appropriate solids phase, Na_2SO_4 with or without hydration and the sodium sulfate carbonate double salt, $Na_6(SO_4)_2CO_3$. Work on database development is being performed with the Task associated with Saltcake Dissolution, 3.2. Samples have been prepared for total inorganic carbon (CO_3^{-2}) analy-

sis and a comparison of these results with the model predictions will be reported later.

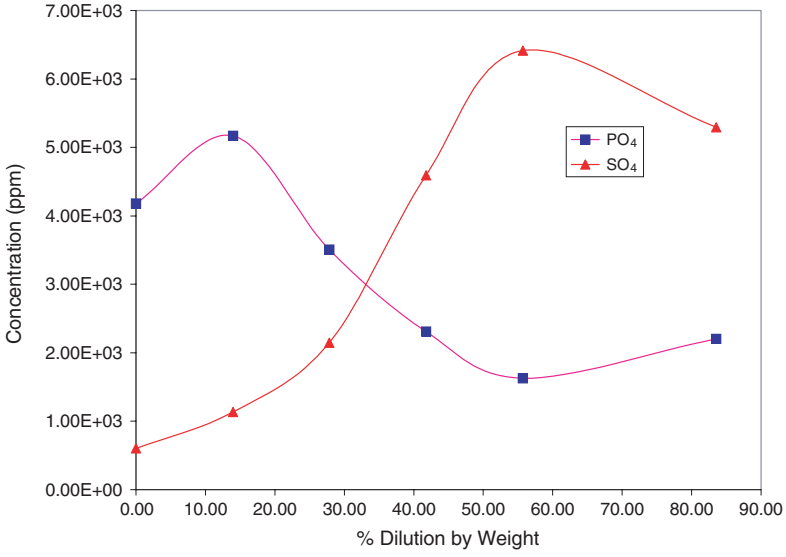

FIGURE 22. ESP predicted concentrations for phosphate and sulfate anions as a function of diluent added.

Although additional comparisons are needed along with model calculations, the comparison between the experimental results and the model for the initial surrogate saltcake supernatant are seen to be in excellent agreement for sulfate, nitrite and nitrate, Table 3. Differences in the phosphate likely reflect that refinements are needed to account for the partitioning of the phosphate in the solid phase. Similar comments apply to the dissolution of the sulfate containing particles. The standard deviations and standard deviation errors associated with the experimental data confirm that the composition of the col-

umn effluent is not changing over the first 630 minutes or 10 and 1/2 hours of the experiment.

TABLE 3. ESP predictions, average concentrations, standard deviations, and standard deviation errors for the concentrations in Figures 19 and 20 to a run time of 630 minutes.

	PO_4^{-3}	SO_4^{-2}	NO_3^{-1}	NO_2^{-1}	$Al^{+3(a)}$
ESP	4.18E+03	6.02E+02	8.58E+04	1.01E+05	2.58E+04
Average	1.46E+03	8.90E+02	9.35E+04	9.92E+04	4.83E+04
Std	7.63E+01	8.16E+01	1.31E+03	1.63E+03	2.60E+03
STD Error (%)	5.21	9.17	1.40	1.64	5.38
(a) It is believed that ICP matrix effects are responsible for the differences observed with aluminum. These effects are under investigation.					

The performance of additional experiments is currently underway to achieve a run whereby channeling due to mechanical means as opposed to any natural channeling within the saltcake can be distinguished. Additional pressure transducers have also been ordering such that the porosity and permeability of the saltcake composition can be determined as a function of time.[26]

Studies on Particle Transport

Work has previously been presented in this sequence associated with the evaluation of particle deposition during slurry waste transfers.[24] Previous work at Hanford has resulted in schedule slips and additional infrastructure investments owing to pipeline plugging and the difficulties in remediating plugs such that waste could be efficiently and safely moved. In light of the operational difficulties it was determined that additional computational fluid dynamic calculations were needed. The calculations have been performed in an attempt to isolate the primary factors responsible for particle deposition.

The simulated channel diameter was taken as 7.62 cm (3 in.) and the length of the pipe was set at 11 m. The computation grid consisted

of 22 cells in the *z* (flow axis) directions, 10 *y* cells from the top to the bottom of the channel, and 10 cells in the *x* direction. A cylindrical-polar coordinate grid was used. The two-phase flow model used in the results given below is denoted as the algebraic slip model (ALSP). The model is capable of accounting for up to 100 different sizes of particles but in these calculations any distribution effects were, as determined from previous work, neglected.[24] The model is capable of predicting deposition and fluid flow but is not suitable for quantifying changes in local process chemistry such as would occur during crystal growth associated with saltwell supernatant or evaporator brine transfers).

Initially the main goal of the simulations was the direct determination of the critical velocity followed by comparison to existing phenomenological expressions. A number of relationships have been advanced to describe the onset of particle sedimentation in laminar and turbulent flow fields; however, many of these expressions provide conflicting results for the same flow conditions. As shown below it is believed that the simulations reported here are resulting in the determination of a transition velocity that describes the change from a moving bed flow to the onset of particle pile-up. In conventional descriptions of two-phase fluid dynamics the initial point where a particle undergoes deposition is referred to as the critical velocity. Groups of particles will then settle and depending on the stream velocity may be pushed along with the flow. This would signify the moving bed stage. As the velocity is reduced the drag on he particles will exceed the forward momentum thereby resulting in slip which ultimately and at low velocities will result in the beginning of a particle pile which for practical purposes would signify the initialization of distinct plug formation.

Simulations were performed for a given particle diameter and mixture density and viscosity as a function of inlet velocity. The volume fraction of the particles was always set to 0.1. Figure 23 is a two-dimensional, centerline plot of the particle loading through the pipe.

In this and subsequent figures the channel diameter has been scaled by a factor of 50 and the 11 m length of the pipe has been reduced accordingly. The scale on the left hand side of the plot indicates the particle loadings.

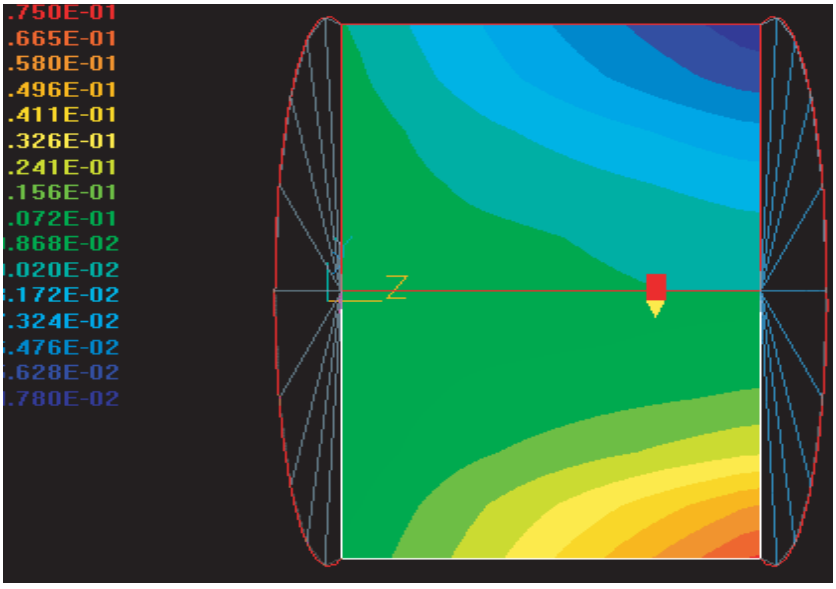

FIGURE 23. Centerline particle loading profile for a simulation with 100 micron diameter particles, a mixture viscosity of 4 cP, a reduced density of 1100 kg/m^3, a particle volume fraction of 0.1 at a velocity of 0.80 m/sec.

The plot indicates that although deposition is occurring the particles are not tending to congregate within the lower portion of the channel away from the exit. This indicates that the velocity employed for this specific simulation is sufficient for transport of the particles through the 11-m distance. Reducing the inlet velocity results in additional deposition, Figure 24, until at lower velocities, Figures 25 and 26, increased particle loadings are observed at intermediate distances along the pipe.

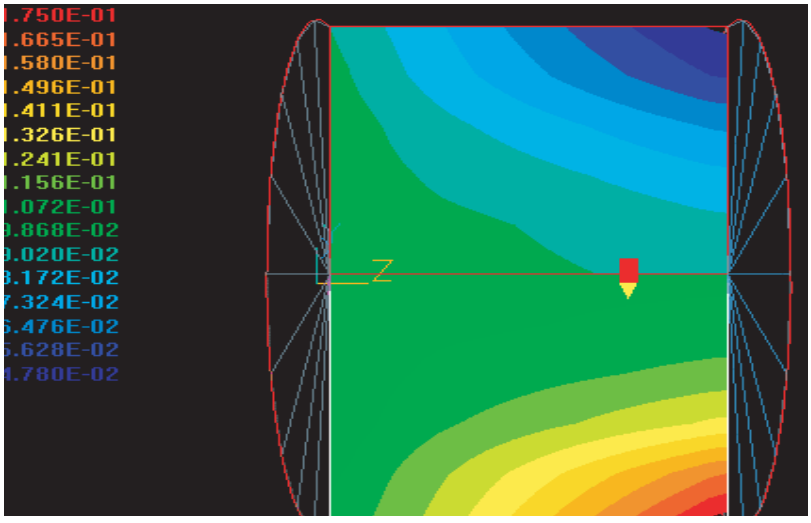

FIGURE 24. Exactly as in Figure 23 but with an inlet velocity of 0.7 m/sec.

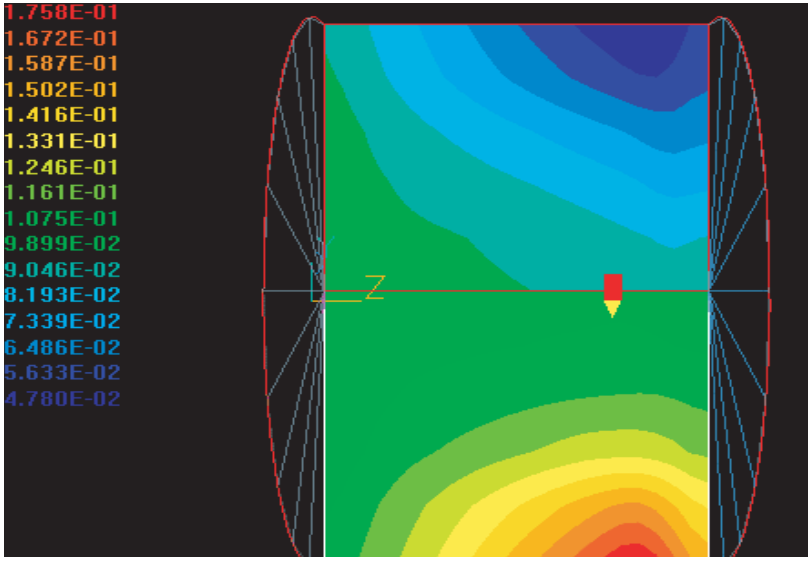

FIGURE 25. Continued study of the slurry composition of Figures 23 and 24. Here the inlet velocity is 0.6 m/sec.

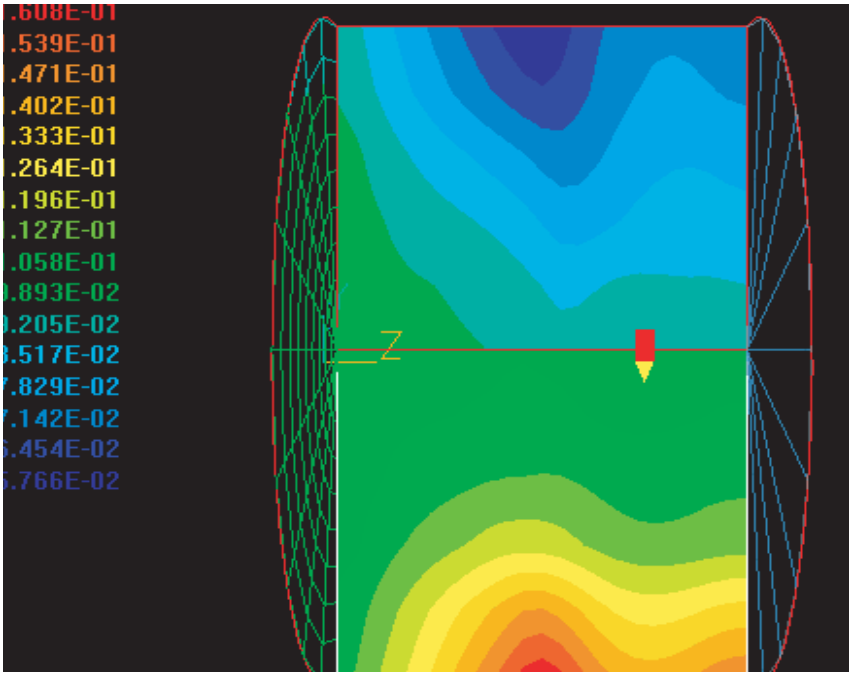

FIGURE 26. As in Figures 23, 24, and 25 with an inlet velocity of 0.45 m/sec.

Reduction of the inlet stream velocity is accompanied by a shift in the particle loading in the lower portions of the pipe toward shorter distances. This observation suggests that a plot of the particle loading near the bottom of the pipe against the distance along the channel would serve for determination of the velocity where the flow transitions from that of a moving bed to a particle pile.

Figure 27 illustrates this approach. These results are for flow another simulation, see below, and provide a somewhat finer determination of the transition velocity than can be visually inferred from the contour plots. The volume fraction is a linear function of the distance along the particle channel until the inlet velocity becomes 1 m/sec. It then becomes possible to interpolate between the linear and non-lin-

ear profiles to determine the value of the transition velocity. For the data in Figure 27 the transition velocity is 1.05 m.sec.

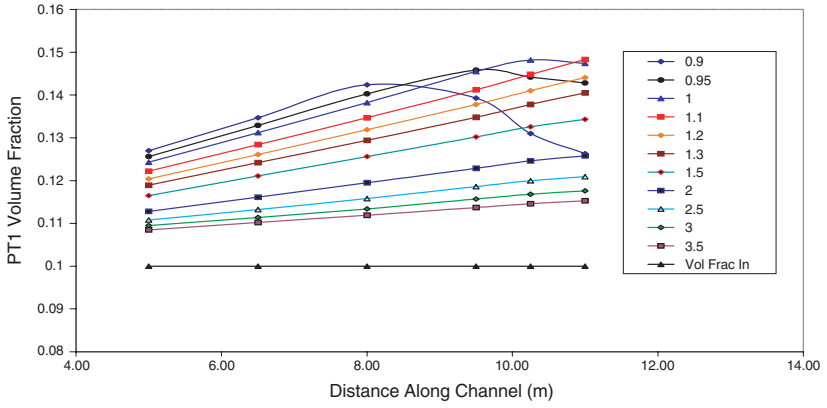

FIGURE 27. Determination of the transitional velocity for a base simulation with 50-micron particles, a 9 cP mixture viscosity, a particle density of 5000 kg/m^3, over an 11-m distance. In this and all other simulations reported here the particle volume fraction was kept at 0.1.

Simulations were conducted for different particle diameters ranging from 25 to 200 microns and for reduced density values of from 1 - 4. Here the reduced density was defined as the difference of the particle density minus the carrier fluid density over the carrier fluid density. The density of the medium was assumed that of water and taken as 1000 kg/m^3. Results for these simulations are collected in Table 4 and in the figures that follow.

TABLE 4. Simulation transition velocities and slurry parameters. All runs correspond to the 11-m long, 7.81-cm diameter channel at 25 C.

Particle Diameter (microns)	Reduced Density	Mixture Viscosity (cP)	Transition Velocity (m/sec)
50	1	4.00	0.38
100	1	4.00	0.65

TABLE 4. Simulation transition velocities and slurry parameters. All runs correspond to the 11-m long, 7.81-cm diameter channel at 25 C.

200	1	4.00	1.18
25	2	9.48	0.30
50	2	9.48	0.56
100	2	9.48	1.03
150	2	9.48	1.46
200	2	9.48	1.83
50	4	9.00	1.05
100	4	9.00	1.78
150	4	8.80	2.31
200	4	9.00	2.88
250	4	8.80	0.58

The data in the table indicate that all three parameters could influence the transition velocity. In order to separate the effect of the mixture viscosity from that of the reduced density and the particle diameter a study was conducted where the later two parameters were kept constant and the viscosity was varied. Figure 28 is a plot of the determined velocity against the viscosity. Here the particle diameter was 100 microns and the second phase density was 3000 kg/m^3.

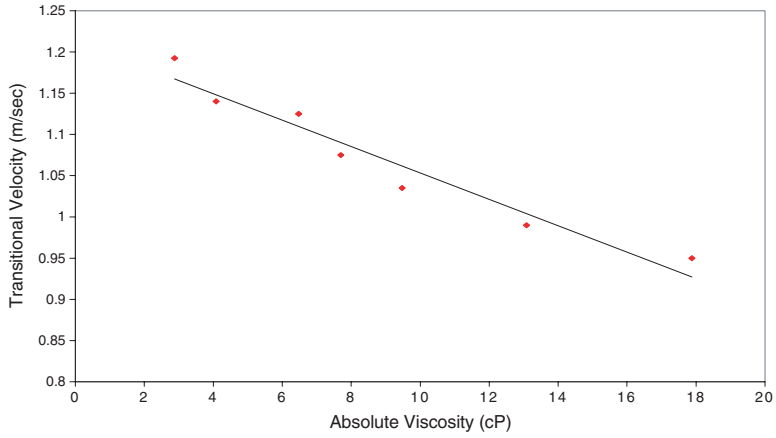

FIGURE 28. Effect of the mixture viscosity on the transition velocity.

A line describes the data and the velocity depends upon the mixture viscosity according to

$$V_{trans}\,(m/sec) = -1.6 \times 10 - 2\eta + 1.2 \qquad \textbf{(EQ 3)}$$

Changing the viscosity from 2.9 to 17.9 cP results in a decrease of the transition velocity from 1.19 to 0.95 m/sec; a 620% increase in the viscosity amounts to only a 20% change in the velocity. The decrease in the velocity with an increase in the viscosity corresponds to an increase in the buoyant force applied to the particle.

Velocity trends on the reduced density and the particle size can be developed from the data in Table 4. Values of the determined parameter are shown plotted against particle diameter at different reduced densities in Figure 29. The expressions given in the figure allow for a determination of the sensitivity of the transitional velocity upon the average particle diameter. For all densities it was determined that a 1% change in the particle diameter corresponds to a 0.8% change in the determined value of V_{trans}. Similarly, the sensitivity of the transitional velocity with reduced density was determined. A 1% change in the reduced density was found to result in a 0.8% change in the tran-

sitional velocity. The simulations indicate that the primary physical parameters that affect the transitional velocity are the particle diameter and the reduced density. A 1% change in the slurry viscosity only amounts to a 0.03% change in V_{trans}.

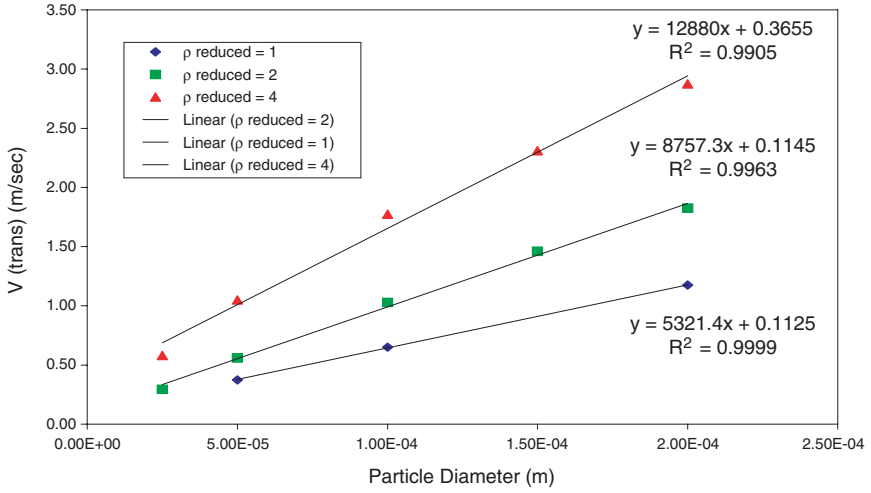

FIGURE 29. Values of the transitional velocity plotted against the average particle diameter at different values of the reduced density.

In order to frame the previous work the results were compared to a number of different expressions for the critical velocity. As already discussed it is believed that the simulations do not provide the critical velocity but rather a transitional velocity relating to the change from a moving bed flow to particle pile-up. Still it is instructive to examine the various expressions in light of correlations to existing phenomenological expressions used at Hanford. Table 5 provides the results of

the ALSP calculations along with some selected expressions for same values of the parameters used in the simulations.

TABLE 5. Comparison of the transition velocities from the simulations with calculated critical velocities from a number of different empirical expressions. All velocities are in m/sec.

Designation	V_{trans}	Shook	Spells	Wasp	Hudson	Oroskar & Turian (a)	Durand
50 9 cP	1.05	0.89	0.46	1.46	1.69	1.82	3.67
100 9 cP	1.78	1.43	0.81	1.64	2.84	2.02	3.67
150 8.8 cP	2.31	1.83	1.13	1.76	3.85	2.14	3.67

It is important to note that the critical velocity is that velocity at which particle sedimentation begins and that vast differences exist among the various predictions. Calculated critical velocities from the expressions of Wasp, Hudson, Oroskar and Turian, and from Durand are all larger than the values of the transition velocity predicted from the simulations. The increased values lend credence to the flow field simulation results. Specifically the critical velocity should be larger than the velocity where the flow changes from a moving bed to particle accumulation. Results from the expressions of Shooks and from Spells are less that those predicted by the simulations and as such are not believed to directly reflect the flow field.

The expression used by Hudson was employed to design the Hanford cross-site transfer line. Based on the ALSP simulation results presented above operating at velocities greater than those predicted by the Hudson equation would not expect to lead to particle sedimentation and eventual plugging.

During the performance of this work additional results from particle size distribution measurements at Hanford have become available.[27] These data indicate somewhat reduced diameters compared to those employed in the simulations. Additional simulations are in

progress to further track the flow hydrodynamics at particle diameters down to 10 microns. Furthermore, simulations have been started using a second model for two-phase flows.

Project Status

Work is continuing on both the saltcake dissolution flow module experiments and on simulation support for Hanford waste transfers.

Conclusions

The initial experiments with baseline saltcake surrogate dissolution in the SDFM have indicated that a significant length of time is required for the effect of the diluent on the saltcake to be observed. During this ten-hour period the effluent viscosity was observed to remain at or very near that measured on the un-diluted surrogate supernatant. Thereafter a second region is observed wherein the viscosity is reduced and the chemical composition of the effluent changes. Nitrate, phosphate, and sulfate anion concentrations increased in accordance with dissolution of their respective salts. Aluminum and nitrite concentrations were reduced and this behavior is associated with the direct dilution of the soluble nitrite anion and with the formation of gibbsite from aluminum hydroxide as the pH of the liquid phase is reduced by the addition of the diluent. Results for the supernatant viscosity and the nitrate, nitrite, and sulfate anions are in agreement with the predictions from the ESP model. Direct comparison to the model predictions indicated that only a 14% (by weight) extent of dilution was observed. Additional work is in progress to streamline the experimental operations and to extend the dilution of the baseline surrogate.

CFD simulations on slurry transport have indicated that a flow regime consistent with the critical slowing down of a moving particle bed eventually leading to an accumulation of particles can be deter-

mined. The associated transition velocities were found to be linear function of the average particle size and reduced particle density and the slurry (mixture) viscosity. Of these parameters the particle diameter and reduced density were found to influence the transitional velocity to a much greater extent that the slurry viscosity. Nominally a 0.8% change in either the particle diameter of density results in a 1% change in the determined velocity. A 620% change in the mixture velocity was only observed to result in a 20% change in the transition velocity. Comparison of the determined velocities with empirical expressions for the critical velocity, defined as that velocity at which the particle begins to undergo sedimentation, has allowed an initial assessment of the applicability of these expressions. The expression developed by Hudson and used to design the cross-site transfer line at Hanford results in a critical velocity 60% larger than the transition velocity obtained from the CFD simulations. The increase in this value lends credence to the use of the expression in Hanford design studies, as the critical velocity must be considerably larger than the transition velocity. Based on the simulation results operations at the Hudson critical velocities would not result in particle pile up or the eventual formation of a pipeline plug.

Work Planned

Further experiments and ESP simulations will be performed on the Saltcake Dissolution Flow Module. The short-term goal is to complete an experiment for the baseline surrogate wherein only channeling from the dissolution process is occurring. Thereafter a second formulation will be examined. Experiments will be conducted with saltcakes of different liquid phase volume fractions. In this way the extent of moisture within the salt matrix can be correlated with the porosities and chemistries that may be more representative of salt wastes that have remained with the Hanford single-shell tanks for some time.

Additional ALSP simulations and correlations will be performed to extend the results to particle sizes currently believed to be more appropriate for Hanford slurries. It is not believed that the main conclusions from the simulations presented here will change at lower particle diameters; however, the additional calculations will extend the range of the simulations such that they encompass all of the possible conditions that could be anticipated. Further reduction of the simulation results and more formal comparisons with those critical velocity expressions that appear to make sense will be performed. Additionally simulations are in progress with a second two-phase flow model that will permit the incorporation of heat transfer and also allow for changes in the chemistry of the stream to be accounted for.

References

23. D.A. Reynolds. May 2000. Status of waste transfers, criteria, and plans. Presented at the 3rd Saltcake Dissolution and Feed Stability Workshop, Richland WA, and

J.R. Jewett. January 2000. “Tank Farm Information for TFA Workers” and” Saltwell Pumping from Tank SX-104,” Numatec Hanford Corporation, Richland, WA, personal communication.

24. J.S. Lindner, T. Durve, V. Raju, and R. K. Toghiani. 2001-02. Prevention of solids formation. In DIAL Quarterly Reports 11, 12, 13, and 14, (2001-2002).

25. R. Hunt. Personal communication.

26. M.J. MacDonald, et al. 1991. *AIChE Journal* 37:1583.

27. J.R. Jewett, et. al. March 2002. Values of particle size, particle density, and slurry viscosity to be used in waste feed delivery transfer system analysis. RPP-8085, Office of River Protection, Richland, WA.

TASK 4 *Environmental Control Device Testing*

Evaluation of HEPA Filter Performance

J. A. Etheridge

Introduction

In 2000, the U.S. Department of Energy (DOE) and the Environmental Protection Agency (EPA) signed a Memorandum of Understanding to combine research efforts to the maximum extent possible to resolve important questions of common interest. One of these revolved around the issue of assuring the performance of HEPA filters used in off-gas systems. As a result, this Technical Working Group was chartered to provide methodology to ensure that HEPA filters provided adequate protection throughout their service life. The work proposed here is a direct result of the efforts of the NTW.

One of the major parts of this project is a survey of what has already been done, what is currently being done, and what the priorities are for additional work that needs to completed. At present there is a lot confusion and misinformation concerning HEPA filters, filter testing, and filter applications. There appears to be a strong need for a HEPA filter test bed for the purposes of challenging the filter medium as well as for development of instrumentation. We plan to construct a

filter test bed (HEPA Filter Challenge Facility). It will be capable of DOP/PAO testing as well as handling a variety of other challenge agents including water, smoke, heat, and particles from particle generators. It will be instrumented and monitored in much the same way as the combustion test stand and will also be useful for instrument development and CEM testing. Modeling of the results of specific types of failures will also be done along with testing, where practical, to verify that the model is useful. This is important for understanding both DOP testing and online failure of HEPA filters.

One of the major needs related to HEPA filters is the need for a "break through" detector. Testing of the cavity ring down system for possible use as a break through detector is also planned. It is also proposed to acquire an "electrostatic impactor" (ELPI) for use as both a measure of input challenge agents and for measuring after the HEPA filters. If this unit is successful in measuring very low particle concentrations (or low mass loading) it will allow us to test the limits of detection of other particle measuring techniques.

The scope of this project could be amended depending upon the results of the NTW's review of our Data Quality Objectives and the evolution of the NTW's HEPA Filter Performance position paper. However, it is believed that the activities described below accurately represent the magnitude of the effort, and the equipment and supplies required for the program.

Work Accomplished

The test matrices for Sections 4, 5 and 6 were developed as Excel files. These files were presented to HEPA National Technical Work Group and discussed during a conference call on February 11, 2002.

Preparation of the laboratory for checkout of the particulate instrumentation and calibration testing was completed. Particulate measurement instrumentation, including the ELPI, SMPS, and aero-

sol generators have been set up in the laboratory and interfaced to Laptops and tested. Calibration data is being generated. These data will be included in a paper and presentation being made at the IT3 Conference in New Orleans during April.

Deposition 2001, which is a program distributed by Texas A&M that simulates the deposition of particulates in sample lines or pipes, was acquired. The program allows for the definition of three different particle distributions: monodisperse, polydisperse-lognormal, and polydisperse-user defined. By specifying the desired system properties and parameters one can model particle penetration and deposition. This software will be used to simulate the deposition of particulates in probes and the HEPA test stand.

The preliminary design work for the large particle generator to be used with the test stand was initiated. ASHRAE Standard 52.2 was used as a guide in the design work. The large particle generator will be necessary in order to produce the proper size range of aerosol particles for the test stand. The size of the particle generator will be approximately 2.5-ft diameter and 6-ft tall. This size will allow the particles sufficient time to dry before entering the test duct. The air flow rate in the test duct will range from 50 cfm to 375 cfm.

Sampling System for Dioxins, Furans and Other Semi-volatile Products of Incomplete Combustion and Characterization

C. Waggoner and C. B. Winstead

Introduction

Selected congeners of the families of dioxins and furans (D/F) are potentially some of the most carcinogenic compounds known to exist. Recognition of the potential risk to the U.S. population spurred the conduction of a national inventory of D/F sources. A significant outcome of this initiative has been the establishment of a strategy to reduce emissions in a targeted fashion. One of the centerpieces of the D/F reduction strategy is the Maximum Achievable Control Technology (MACT) standard just issued for hazardous waste combustors (HWC). Each of the DOE hazardous or mixed waste incinerators falls subject to this new standard and there are stringent emission levels that will need to be met in the near future.

The 0.2 ng/dsm^3 emission standard called for under the HWC-MACT stresses the technical limits of operational control and emissions testing. Uncertainties associated with US EPA reference

method stack sampling accuracy and method quantification limits for the 17 D/F congeners that have non-zero toxicity equivalence factors invite skeptical review of the measurements that will be made by facilities to demonstrate compliance with this new standard.

Of the six needs listed on the DOE EM-Needs web page related to dioxin/furan problems, three (ID-3.2.32, ID-S.1.02, and SR00-1021) recognize the lack of knowledge associated with the specific locus of D/F formation, the distribution of D/F congeners between adsorbed and gaseous phases at temperature, and/or the behavior of these classes of compounds in the sampling train. This lack of knowledge is an impediment to minimizing emissions by process control or design/operation of pollution control devices. Additionally, a much fuller understanding of the phase behavior in off-gases is essential to development of a functional continuous emission monitor or verifying the accuracy of extractive sampling methodologies. Finally, a clearer picture of the gas phase chemistry is the best hope of identifying a dependable analytical surrogate, if one exists.

Intensive research has been undertaken throughout the past two decades to gain a more complete understanding of the mechanism(s) of dioxin/furan formation in combustion processes. The majority of controlled mechanistic studies of D/F formation tend to be carried out using bench top and micro-scale apparati. A significant body of data has also been accumulated from off-gas samples collected from solid waste incinerators and industrial processes. However, the large number of variables associated with fuel feed and operational history of incinerators makes it difficult to extrapolate from bench to full scale. A series of studies is proposed to take advantage of bench scale results and, in a two-stage manner, extend these investigations to pilot scale.

The primary focus of this effort will be to determine the behavior of D/Fs associated with fly ash particulates in an isothermal off-gas environment for the temperature range of 300 to 800 F. This will

include analysis of samples for D/F homologues to determine the extent of formation, destruction, and dechlorination under test conditions.

Work Accomplished

The system has undergone several changes to improve the functionality, but that also delayed progress for a short period of time. The GC oven previously expected to be used as a filter box has now been replaced by a custom made oven from Apex instruments. The GC oven was difficult to control, and in attempting to connect the controller to the computer, some wiring errors were made, and the oven is no longer functional. Repairs likely could have been made, but in light of the fact that the ideal oven would be much larger, a new one was designed and ordered. The new oven is much taller, and is capable of containing the three-way valve along with the filter housing, purge gas line, and necessary fittings, but also can fit an impactor in addition to all of that if needed. Having the valve inside the oven reduces the amount of heating tape needed for the project, and also keeps the amount of the system that is exposed to a minimum.

Prior to the new oven being ordered, some modifications had been made to the system. The particle feeder was wired to the computer so that the motor in the feeder could be monitored and controlled by the same software program that controls the gas flow rates and the heater temperatures. The motor is currently being calibrated to specific particle feed rates.

Temperature controllers for the system have arrived and been tested. Further testing will be necessary when all of the controllers and their respective devices are set up for a run. The controllers have been moved to a central location and arranged in a more convenient setup for adjusting the system if necessary. The new oven came with a controller, and plans are being made to connect it to the computer software.

The power supply has been fitted with a power switch, and is in the process of being wired to a controller so that the temperature of the peltier coolers can be monitored. The studies on the trap have not been completed. It has been proposed that a trap of greater surface area be constructed to increase the cooling and heating rates.

The machine shop has manufactured a brace for the three-way valve. Since it is an all metal valve, opening and closing it requires a lot of force. The brace is designed to prevent unnecessary stress on the fittings and tubing surrounding the valve. The brace was designed for the previous oven, but should be able to be modified for the new one.

Work Planned

DIAL will continue to develop its small-scale test stand for D/F research and the evaluation of its isokinetic and isothermal sampling system. During the next three months emphasis will be placed on completion of the assembly of the sampling system components with respect to thermal and flow properties. Testing will begin to ensure that the entire system functions as desired, considering both temperature and flow requirements. The system will then be sent to Restek to be coated with the inerting material. Other issues that need to be addressed include reducing the carrier gas flow rate for the particle feeder to a level that is functional with regard to particle transport and nominal with regard to perturbing the off gas chemistry and temperature profile in the region downstream of particle injection.

References

28. K.L. Froese, O. Hutzinger. 1997. *Environmental Science and Technology* 31:542-547.

29. A. Addink, H.A.J. Govers, K. Olie. 1998. *Environmental Science and Technology* 32:1888-93.

30. P.M. Lemieux and J.V. Ryan. 1998. *Waste Management* 18:361-370.

31. P.H. Taylor and B.J. Dellinger. 1999. *Analytical and Applied Pyrolysis* 49:9-29.

32. F. Iino, T. Imagawa, M. Takeuchi, M. Sadakata. 1999. *Environmental Science and Technology* 33:1038-43.

Toxic Organic Compound Monitoring Using Cavity Ringdown Spectroscopy

C. B. Winstead

Introduction

Several US DOE science and technology needs are based upon the need for high-sensitivity and robust monitoring devices for various organic species. For example, the following needs are all related to the monitoring of volatile or semi-volatile organic compounds (VOCs or SVOCs) in combustion or thermal treatment systems:

- Continuous Emissions Monitor for Offgas Analysis (ID-2.1.18, Priority 1)
- Develop Thermal Treatment Unit Offgas CEM Monitors (ID-3.2.32, Priority 2)
- Volatile Organic Compound Monitoring and Detection (ORHY-04, Priority 3)

The effort reported here is a continuation and combination of two separate tasks from DIAL's previous cooperative agreement (Task 1.1 *Volatile Organic Compound Monitors Using Diode Lasers* and Task 1.3 *Sensitive Detection of Toxic Chlorinated Compounds*). Together, these projects have demonstrated the first sensitive detection of VOCs such as benzene and chlorobenzene using diode laser CRDS and

obtained the first CRDS spectra for dioxin (an SVOC). While the emission of dioxins and furans are important risk and regulatory drivers, significant research will be required prior to full development of a dioxin/furan continuous emission monitor (CEM). Questions such as how dioxin is partitioned in the gas stream between gas and particulate phases must be investigated and appropriate sampling systems developed before truly quantitative analysis can be carried out online. In addition, monitoring dioxin precursor or indicator molecules such as chlorobenzene may prove to be a viable alternative to dioxin monitoring.[33] Thus, it is beneficial for the development of VOC or SVOC monitors for thermal applications to be coupled with an overall investigation of formation and monitoring of dioxin. Such instruments likely will have value in research efforts to understand dioxin formation well before reaching a level associated with an industrial CEM, a role that may ultimately prove more important for reducing dioxin emissions than a commercial CEM.

The approach taken here includes continuing the development of advanced CRDS techniques using both ultraviolet pulsed and near-infrared diode lasers for the detection of VOCs and SVOCs at atmospheric or reduced pressures. CRDS is based upon the measurement of the time required for light to decay in a stable optical cavity.[34] This light may be injected into the cavity using either pulsed or continuous wave lasers. A small quantity of an absorbing species present in the optical cavity will absorb and thus remove some light from the cavity, reducing the decay time. This change in ringdown time can be directly related to the number density of absorbing atoms or molecules in the cavity. The extreme sensitivity of the CRDS techniques is achieved due to the extremely long effective pathlength (up to several kilometers) for the light recirculating in the cavity to interact with a sample gas.

The efforts described here are focused on improving the sensitivity and selectivity of our previous measurements and participating in collaborative efforts to develop appropriate sampling systems for

dioxin species. Slit jet expansion techniques will be incorporated with CRDS to cause narrowing of molecular spectra by decreasing the population in excited vibrational and rotational energy levels.[35] This narrowing will reduce the spectral overlap between different VOCs or SVOCs, thus enhancing detection selectivity. The slit jet expansion will initially be tested with VOCs prior to a demonstration of the detection of dioxin. The expansion cooled spectra will be directly compared to our other room temperature dioxin data to quantify the change in detection limit due to the expansion. These efforts are designed to be complementary to those underway by EPA researchers who are using resonantly enhanced multi-photon ionization (REMPI) for dioxin detection.[36] Continued development of CRDS should ultimately provide a technology complementary to the REMPI system. CRDS sensitivity should not be strongly impacted by increasing chlorination of dioxin molecules, in contrast to expected sensitivity reductions for REMPI.

Finally, small yet ultra-sensitive sensor systems could no doubt play a significant role in monitoring and/or process control for a number of remediation activities related to clean-up of volatile organics. For example, a number of subsurface and ground-water remediation efforts could benefit from on-line "process" monitoring for VOCs. These include efforts utilizing soil heating, in-well vapor stripping, passive soil vapor extraction, and other in-situ clean-up technologies where simple, real-time VOC monitoring could be used to indicate or monitor system performance. Low-power sensing technologies for VOC monitoring will be required for long-term monitoring efforts both for atmospheric and subsurface monitors, e.g., for continuous monitoring of subsurface reactive barriers or VOC plumes. Systems have already been demonstrated that utilize underground piping to collect soil gas and transport it to a surface monitoring system.[37] For long-term monitoring, diode-based VOC monitoring systems could significantly simplify the analytical equipment required for monitoring while reducing power consumption, features important for use in remote locations. Our continued development of diode laser CRDS

may impact these areas in addition to thermal or combustion system monitoring.

Work Accomplished

The construction of the vacuum and slit jet expansion system for dioxin monitoring is essentially complete. The system has been vacuum tested using both the mechanical and diffusion pumps and is achieving pressures down to approximately 10^{-8} torr. Optical breadboards, vacuum bellows, and optical mounts have been added for mounting the ringdown mirrors and the frame has been reinforced for additional stability. The pulsed valve has been installed in the vacuum chamber and is undergoing initial testing. The operating characteristics of the valve (pulse width, physical adjustment of the orifice and solenoid, etc.) must be optimized to allow the expansion to achieve maximum cooling with a minimum of open time for the valve. A lower duration for the valve opening reduces the overall background pressure in the vacuum chamber. The laser system to be used for the slit jet-cavity ringdown measurements has required some additional maintenance and adjustment, and this work continues.

A master's thesis in chemistry was completed and successfully defended in January based on work accomplished with the diode laser cavity ringdown system. Experimental work with the diode laser ringdown system has resumed following the thesis defense. This work is aimed at completing long wavelength scans of the C-H stretching vibration overtones for several volatile organic compounds. At present, the external cavity diode laser system is exhibiting excessive mode hop behavior that is slowing this effort. Unfortunately, the manufacturer of the system has discontinued this product, making replacement parts difficult to obtain. We have attempted to improve the laser performance by installing a new diffraction grating and adjusting the optical alignment of the laser. However, the problem with the laser persists. We are presently discussing the problem with the manufacturer to determine whether or not the

laser should be returned for service. In addition, the gas mixing system and vacuum chamber were utilized for two days for testing metal oxide sensors. The system has been completely reassembled for VOC cavity ringdown measurements and is functioning well using the distributed feedback laser rather than the ECDL.

Work Planned

For the next quarter, efforts for the slit-jet expansion dioxin work will focus on optimization of the pulsed valve performance and the acquisition of initial spectroscopic data for a volatile organic compound. A compound such as benzene will be used to establish appropriate data acquisition procedures and optimize experimental timing between the pulsed valve and the pulsed laser. This effort is necessary to pave the way for future, more complicated efforts using semi-volatile organic compounds such as the dioxins and furans. The use of volatile compounds will allow for the optimization of the experimental conditions without the complexity of the sample introduction procedures required for semi-volatile compounds.

References

33. R. Zimmerman, J.J. Heger, M. Blumenstock, R. Dorfner, K.-W. Schramm, U. Boesl, and A. Kettrup. 1999. On-line measurement of chlorobenzene in waste incineration flue gas as a surrogate for the emission of polychlorinated dibenzo-p-dioxins/furans (I-TEQ) using mobile resonance laser ionization time-of-flight mass spectrometry. *Rapid Communication Mass Spectrometry* 13:307-314.

34. For example,
J.J. Scherer, J.B. Paul, A. O'Keefe, and R.J. Saykally. 1997. Cavity ringdown laser absorption spectroscopy: history, development, and application to pulsed molecular beams. *Chemical Reviews* 97:1:25-51.

G.P. Miller and C.B. Winstead. 2000. Cavity ringdown laser absorption

spectroscopy. In *Encyclopedia of Analytical Chemistry*, R.A. Meyers, ed., pp. 10734-10750. John Wiley and Sons, Ltd., Chichester, England.

35. K. Liu, R.S. Fellers, M.R. Viant, R.P. McLaughlin, M.G. Brown, and R.J. Saykally. 1996. A long path length pulsed slit valve appropriate for high temperature operation: Infrared spectroscopy of jet-cooled large water clusters and nucleotide bases. *Review of Scientific Instruments* 67:2:410.

36. N.B. French, B.K. Gullet, H. Oser, H.-H. Grotheer, and D. Natschke. 1997. Joint DOE/EPA Jet-REMPI Dioxin CEM Test, Final Report.

37. Subsurface Barrier Verification with the SEAtrace™ Monitoring System. U.S. Department of Energy Innovative Technology Summary Report DOE/EM-0549, September 2000.